AFGL-TR-77-0027

ADA039945

MONTE CARLO SIMULATION OF ION
COLLECTION BY A ROCKET-BORNE MASS SPECTROMETER

By

Takashi Sugimura

TRW Systems Group
One Space Park
Redondo Beach, California 90278

Final Report
January 1974 - December 1976

January 1977

Prepared for

AIR FORCE GEOPHYSICS LABORATORY
AIR FORCE SYSTEMS COMMAND
UNITED STATES AIR FORCE
HANSCOM AFB, MASSACHUSETTS 01731

Qualified requestors may obtain additional copies from the Defense
Documentation Center.   All others should apply to the National
Technical Information Service.

REPORT DOCUMENTATION PAGE	READ INSTRUCTIONS BEFORE COMPLETING FORM

1. REPORT NUMBER AFGL-TR-77-0027	2. GOVT ACCESSION NO.	3. RECIPIENT'S CATALOG NUMBER

4. TITLE *(and Subtitle)* MONTE CARLO SIMULATION OF ION COLLECTION BY A ROCKET-BORNE MASS SPECTROMETER	5. TYPE OF REPORT & PERIOD COVERED Final Report. 1/74 through 12/76
	6. PERFORMING ORG. REPORT NUMBER Jan 74 - Dec 76

7. AUTHOR(s) Takashi Sugimura	8. CONTRACT OR GRANT NUMBER(s) F19628-74-C-0128

9. PERFORMING ORGANIZATION NAME AND ADDRESS TRW Systems Group One Space Park Redondo Beach, California 90278	10. PROGRAM ELEMENT. PROJECT, TASK AREA & WORK UNIT NUMBERS 61102F 2310G303

11. CONTROLLING OFFICE NAME AND ADDRESS Air Force Geophysics Laboratory Hanscom AFB, Massachusetts 01731 Contract Monitor: Dr. C. Sherman/LKD	12. REPORT DATE January 1977
	13. NUMBER OF PAGES 63

14. MONITORING AGENCY NAME & ADDRESS*(if different from Controlling Office)*	15. SECURITY CLASS. *(of this report)* Unclassified
	15a. DECLASSIFICATION DOWNGRADING SCHEDULE

16. DISTRIBUTION STATEMENT *(of this Report)*

Approved for public release; distribution unlimited

17. DISTRIBUTION STATEMENT *(of the abstract entered in Block 20, if different from Report)*

18. SUPPLEMENTARY NOTES

19. KEY WORDS *(Continue on reverse side if necessary and identify by block number)*

Monte Carlo
Ion Flux
Free Molecule Flow
Transitional Regime

Debye Length
Plasma Sheath
Rocket-borne probes

20. ABSTRACT *(Continue on reverse side if necessary and identify by block number)*

A systematic parametric variation for the positive ion collection by a rocket-borne probe has been completed for the following parameters; speed ratio 3.10, non-dimensional front face potential -200, zero sidewall potential, Debye numbers from 0.01 to 1000, and Knudsen numbers from 0.007 to 1000. The effects of finite space charge on the vehicle are to lower the ion flux to the stagnation point. It is found that the ion flux follows a uniform trend for Knudsen numbers greater than 0.2, but becomes complicated for the near- → next page

DD FORM 1473 EDITION OF 1 NOV 65 IS OBSOLETE

UNCLASSIFIED

354595

continuum regime, e.g., Knudsen number equal to 0.007, which is discussed in detail. Investigation of vehicle angle of attack and internal degrees of freedom indicate that the effects on the ion flux are small. The formulation for the collection of negative ions has been completed and preliminary results indicate that the electrons are described properly.

ACKNOWLEDGEMENT

iii

TABLE OF CONTENTS

NOMENCLATURE

e	charge on electron
k	Boltzmann constant
m, m_i	mass of neutral molecules, ions
n, n_i, n_e	number density of neutrals, ions, electrons
rd	disc radius
v_m	most probable molecular speed $= \sqrt{2kT/m}$
x	axial coordinate
A_D	disc area
C_I	ion flux coefficient $= N/n_{i\infty} U_\infty A_D$
D	orifice plate diameter
Kn	Knudsen number $= \lambda_\infty/D$
$\dot{N}$	flux of ions
R	orifice plate radius
S	speed ratio $= U_\infty/v_{m\infty}$
T	temperature
U	mean gas velocity in x-direction
λ	neutral mean free path
λ_D	ion Debye length $= \sqrt{kT_\infty/4\pi e^2 n_{i\infty}}$
ϕ	electrical potential
Φ	non-dimensional electric potential $= e\phi/kT$

Subscripts

∞	conditions in free stream
o	orifice plate value
c	corner of flat-faced cylinder
sw	vehicle sidewall

LIST OF ILLUSTRATIONS

1. INTRODUCTION

The objective of the contract "Monte Carlo Simulation of Ion Collection by a Rocket-Borne Mass Spectrometer" has been to establish a connection between the properties of the ambient ionosphere and the strength and chemical state of the flux entering a rocket borne mass spectrometer. The primary concern for this study was the description of the collection of positive ions by a flat faced cylinder, approximately 15 cm in diameter, traveling through a weakly ionized gas. Details of the Monte Carlo direct simulation procedure to predict the collection of positive ions were described by Vogenitz (1973) and Sugimura and Vogenitz (1973,1975) and will not be repeated here. The results presented include a detailed examination of positive ion collection through a systematic study by a variation of the following parameters: Debye numbers of 0.01 to 1000, speed ratios of 0.1 to 5.0, non-dimensional potentials of -10 to -200, and Knudsen numbers of 0.007 to 1000. There have been, however, a number of assumptions that have been relaxed or modified in the present study which will be discussed in detail. For example,

- the effects of the variation of the electric potential on the vehicle have been investigated

- the effects of vehicle angle of attack .

- the consideration of internal degrees of freedom

In addition further extensions of the Monte Carlo method including

- formulation of a procedure to describe chemical reactions

- preliminary calculations to describe the collection of negative ions

will be presented.

2. POSITIVE ION COLLECTION - A SYSTEMATIC PARAMETER STUDY

The vehicle geometry and flow configuration shown in Figure 1 was chosen to represent the shapes currently in use to house rocket-borne mass spectrometers. The front face of the cylinder, the orifice plate, was assumed to be held at a negative potential with respect to the ambient gas, and the positive ion flux induced by the resulting electric field, as well as the density, temperature, and velocity of the ions in the flowfield about the cylinder were computed. The ambient gas was assumed to be composed of neutral molecules, positive ions and electrons. The concentration of ions and electrons relative to neutrals is actually so low in the ionosphere that the former may be considered trace species. Thus, the flow of the charged species will be affected by the neutrals, but not vice versa. Likewise, binary encounters between charged particles can be neglected and the only charged particle interaction arises through the electric field.

The quantity of primary concern is the flux of positive ions to the stagnation point of the cylinder orifice plate. The net current is not of interest; hence the electrons in the gas are of interest insofar as their spatial distribution affects the net space charge. The electrons were prescribed to be an inviscid gas in Boltzmann equilibrium under the electric field. This assumption was shown to be accurate by Vogenitz (1973) for the positive ion collection.

The body geometry considered in this study was a right circular cylinder at zero angle of attack. The electric potential of the face of the cylinder with respect to the ambient gas was specified as an input parameter, whereas the side of the cylinder was assumed to be at zero potential with respect to the ambient gas. This means that the small charge buildup at zero current on the actual flight article (the floating potential) was assumed to be zero. Only that portion of the cylinder side was simulated which was required to compute accurately ion current to the front face.

The hard-sphere interaction law was used for neutral-neutral and neutral-charged particle interactions. The numerical magnitudes of collision cross sections for neutrals and ions were taken to be identical in the present study and the ion and electron temperatures in the ambient gas at infinity were assumed equal to the neutral temperature. The method, however, could treat
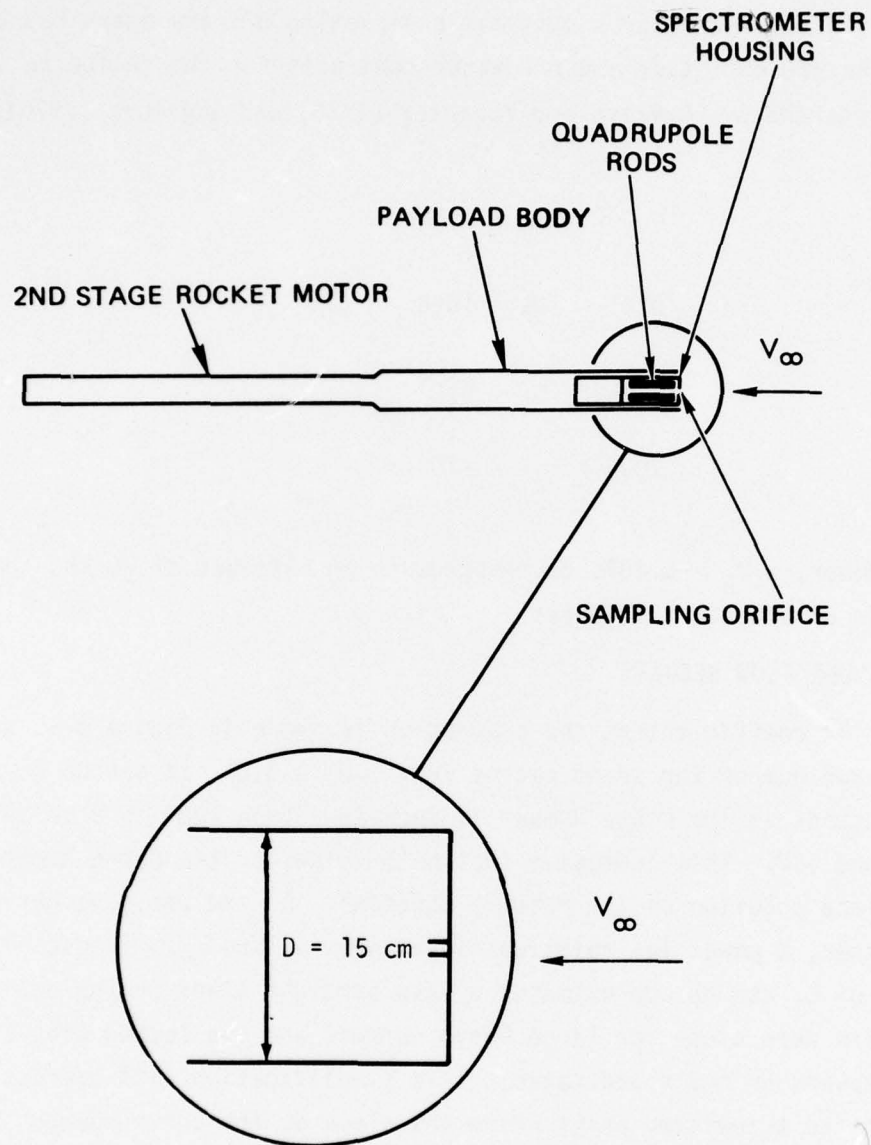
2

TYPICAL SPECTROMETER HOUSING

FIGURE 1

3

arbitrary values of these parameters which are input variables. The effects of varying the speed ratio, front face potential and the effects of different cross sections were discussed by Sugimura and Vogenitz (1975).

In Figure 2, the range of Debye numbers shown as a function of Knudsen number or altitude was taken from Narcisi (1970). This figure shows the expected Debye number range for a given altitude for a vehicle with a 15 cm diameter. As mentioned earlier a systematic variation of parameters has been completed in the present study and predessor contracts for the following values and has been reported by Sugimura and Vogenitz (1975) and Sugimura (1976).

$$0.007 \leq \frac{\lambda_\infty}{D} \leq 1000$$

$$0.01 \leq \frac{\lambda_D}{D} \leq 1000$$

$$0.1 \leq S \leq 5.0$$

$$-200 < \phi_0 < -10$$

The Knudsen number, $\lambda_\infty/D = 0.007$, corresponds to an altitude of 70 km, the lowest altitude of practical interest.

2.1 FREE MOLECULE FLOW RESULTS

The ion flux coefficient at the stagnation is shown in Figure 3 as a function of Debye number for speed ratios from 1.0 to 5.0. It can be seen that C_I is constant as the Debye number is decreased from 1000 to a value between 0.10 and 1.0. This indicates that both values of the Debye number lead to a Laplace solution of the Poisson equation. As the Debye number is decreased further, a power law relationship between C_I and λ_D/D is established. The variation of C_I can be approximated by two straight lines on the semi-log graph. One with zero slope for large Debye numbers and the second with a slope which depends on the speed ratio. This simplification will overestimate slightly C_I at the transition point where the slope of the curve changes but it provides a method for reducing the number of calculations required to determine the Debye number variation. Also shown in the figure is the flux coefficient if the front face potential is taken to be zero. Since the flux coefficient C_I is normalized by the "freestream" flux this value is unity for the free molecule flow limit but is less than unity in the transition regime.
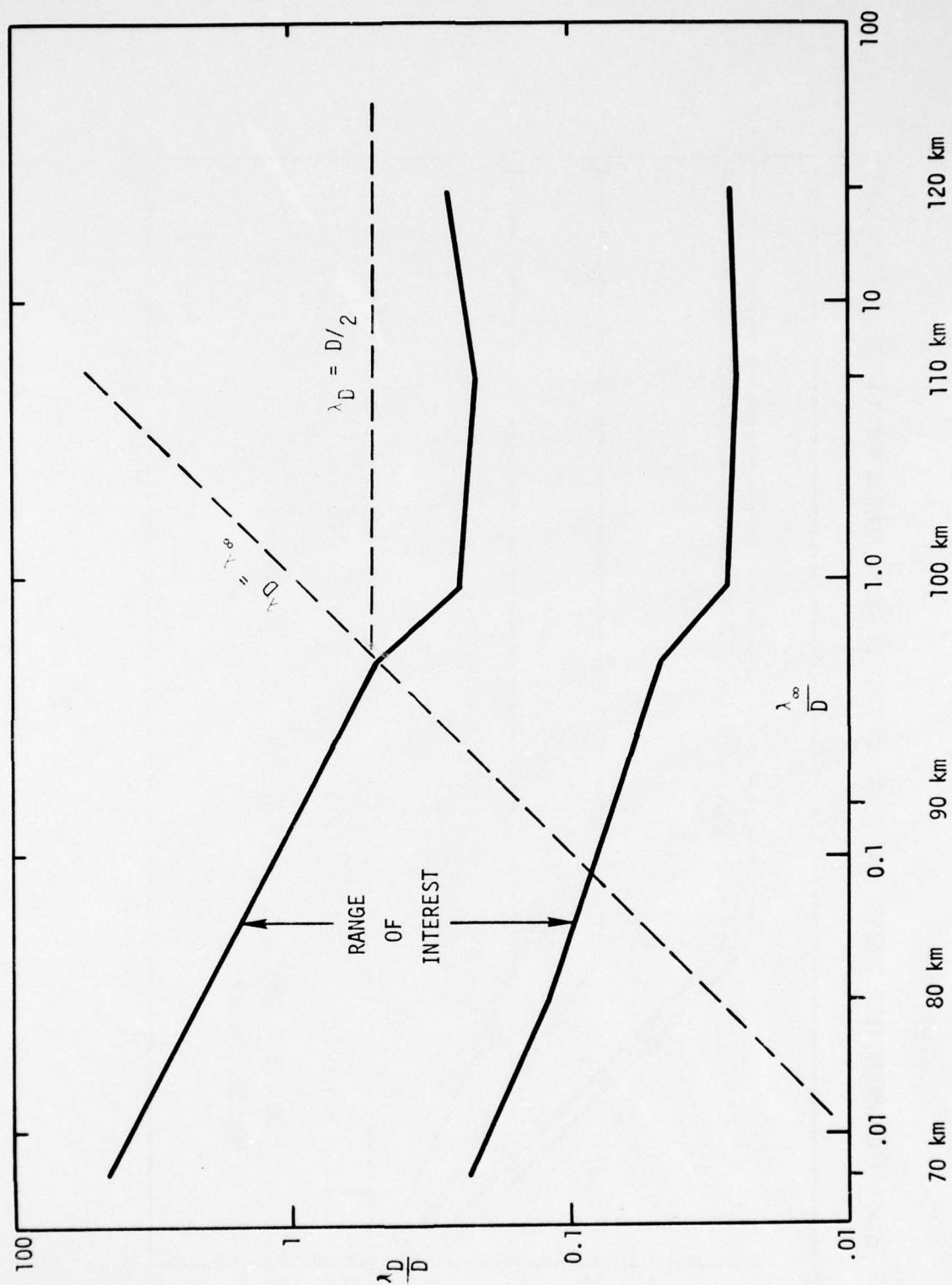
4

LIMITS FOR DEBYE NUMBER WITH ALTITUDE

FIGURE 2

STAGNATION POINT FLUX COEFFICIENT AS A FUNCTION OF DEBYE NUMBER FOR VARIOUS SPEED RATIO
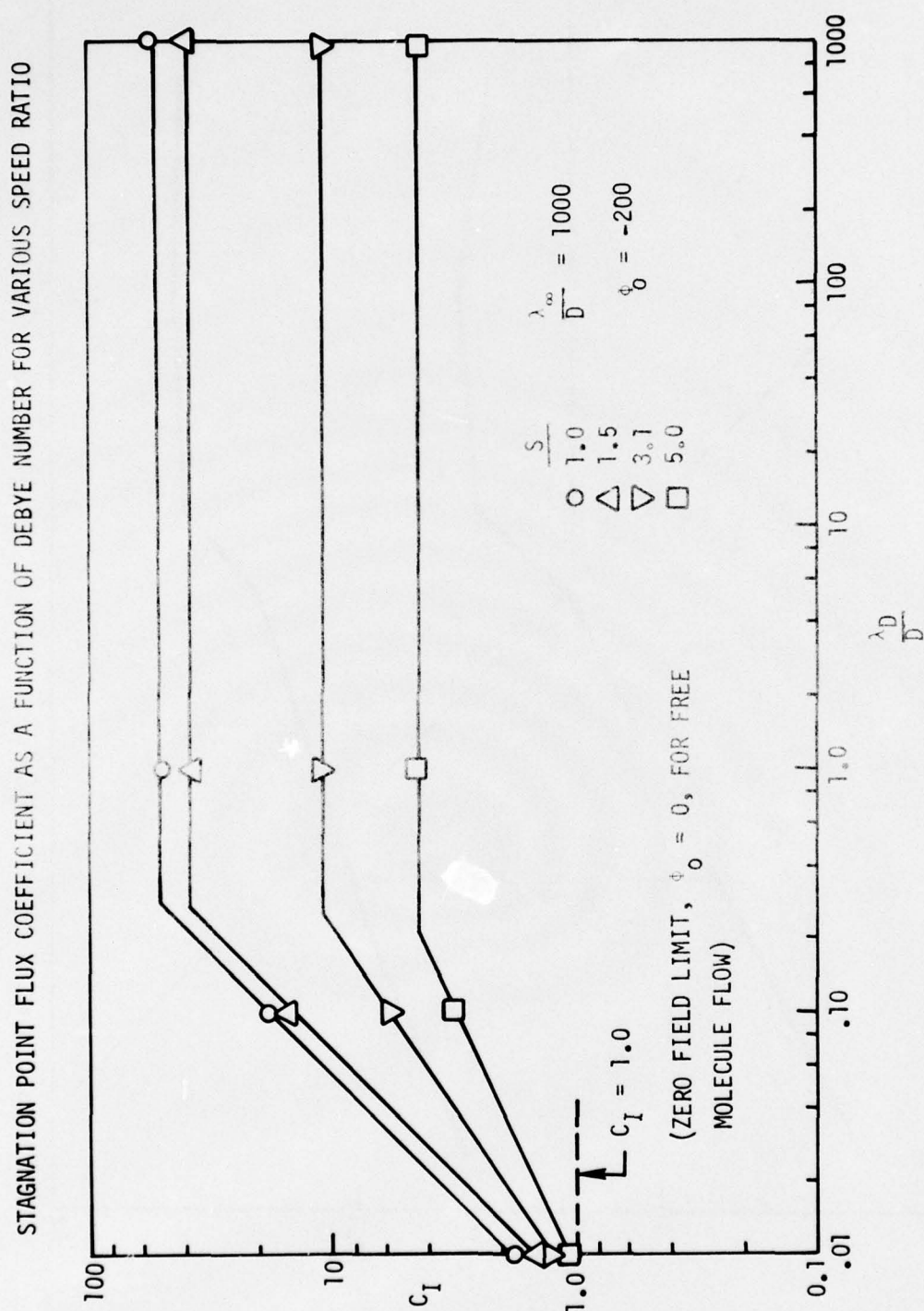
FIGURE 3

In Figure 4 the variation of C_I with speed ratio is shown for Debye numbers from 0.01 to 1000. Again very little difference in C_I is found for Debye numbers 1000 and 1.0. For speed ratios greater than unity a power law variation exists between C_I and S with the exponent depending on the Debye number, λ_D/D. The values of C_I increase rapidly for speed ratios less than unity, due mainly to the fact that C_I is normalized by the freestream velocity.

The previous calculations were all performed with a value of the front face potential equal to -200. In Figure 5 the stagnation point ion flux coefficient is shown to increase linearly as the front face potential is varied from $\phi_0 = 0$ to $\phi_0 = -200$ for a speed ratio of 1.5. These detailed results for a Debye number of 0.1 were presented previously (Sugimura and Vogenitz 1973). If a linear variation of C_I and ϕ_0 is assumed for the other Debye numbers; 0.01, 1.0, and 1000, the dashed lines in Figure 5 result.

The ion flux variation across the front face of the collecting disk is shown in Figure 6 for a Knudsen number of $\lambda_\infty/D = 10$ for Debye numbers from 0.10 to 1000. Also shown in this figure is a result for a Knudsen number and Debye number both equal to 1000. It can be seen that the two results, $\lambda_\infty/D = 1000$ and 10, for a Debye number of 1000 are very similar and represent the collisionless and nearly collisionless cases. The flux for $\lambda_\infty/D = 10$ is slightly lower than the flux for $\lambda_\infty/D = 1000$, which shows the effect of a finite number of collisions. However, the decrease in the flux coefficient at a value of $r_D/R = 0.07$ is due to a small sample size, at least a factor of ten less than the sample size over the entire front face, and the stagnation point flux is found by extrapolating through the other points. A typical sample size at the stagnation point was approximately 3000 particles. The results for a Debye number of 1.0 and 1000 show little difference, indicating again that the Debye number range between 1.0 and 1000 results in a Laplace solution of Poisson's equation. As the Debye number is reduced further, the ion flux coefficient also decreases. For all of these results, the linear variation of the ion flux with radius which characterizes the near-free molecule flow is found again.

In summary, the variation of all the important parameters for the collisionless case are represented on Figures 3 through 6. The speed ratios from 0.1 through 5.0 and Debye numbers from 0.01 through 1000 appear to cover the values

7

STAGNATION POINT ION FLUX VARIATION WITH SPEED RATIO
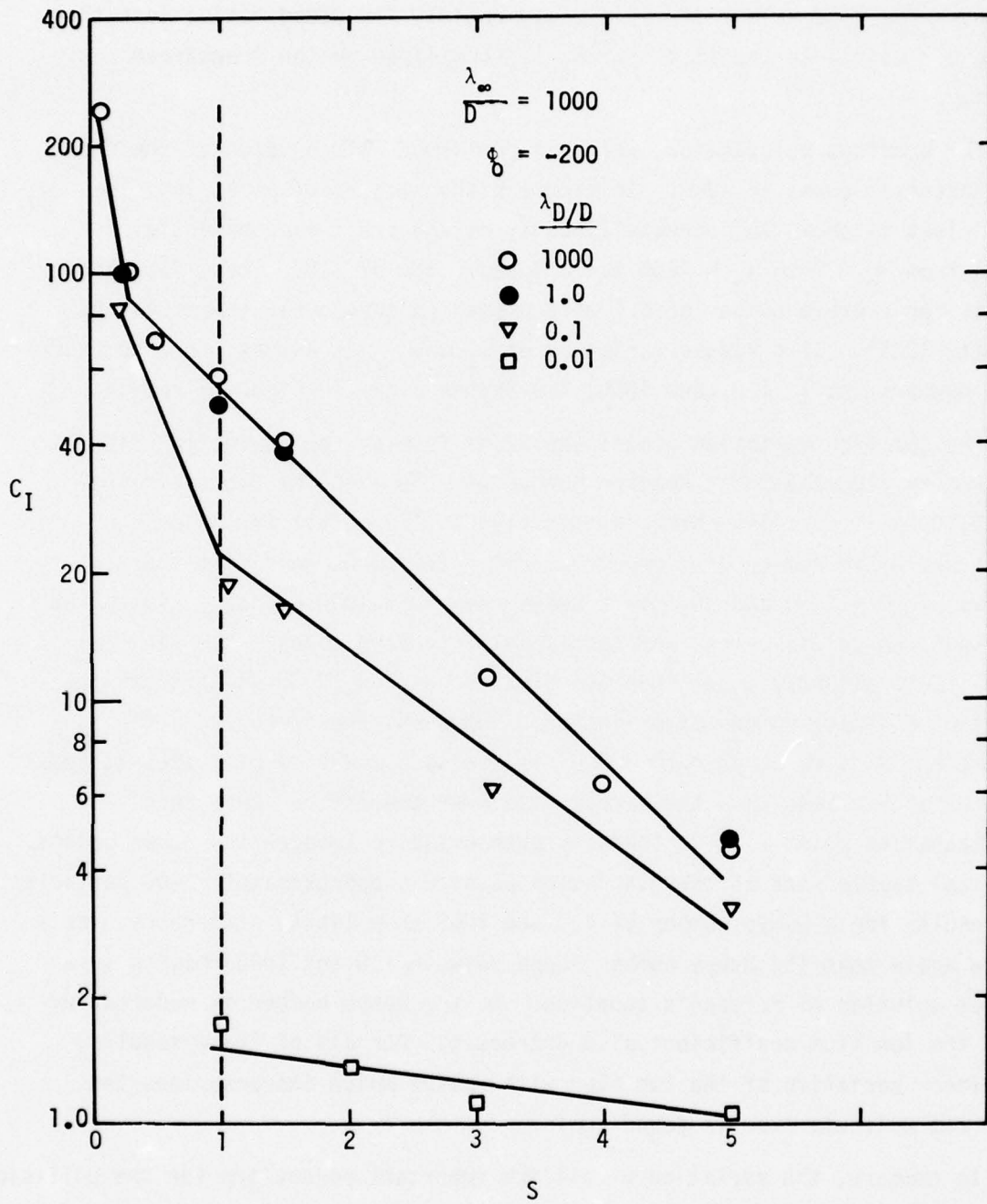

FIGURE 4

STAGNATION POINT ION FLUX VARIATION WITH POTENTIAL

FIGURE 5

9

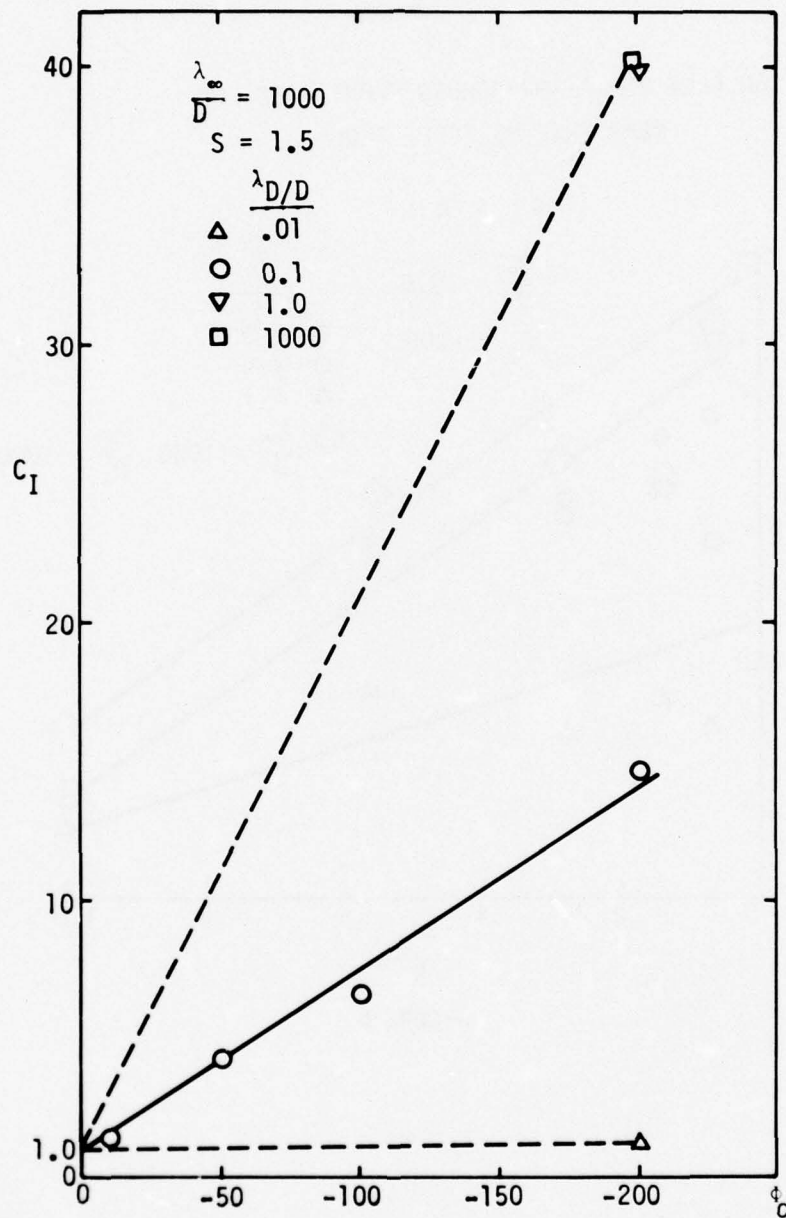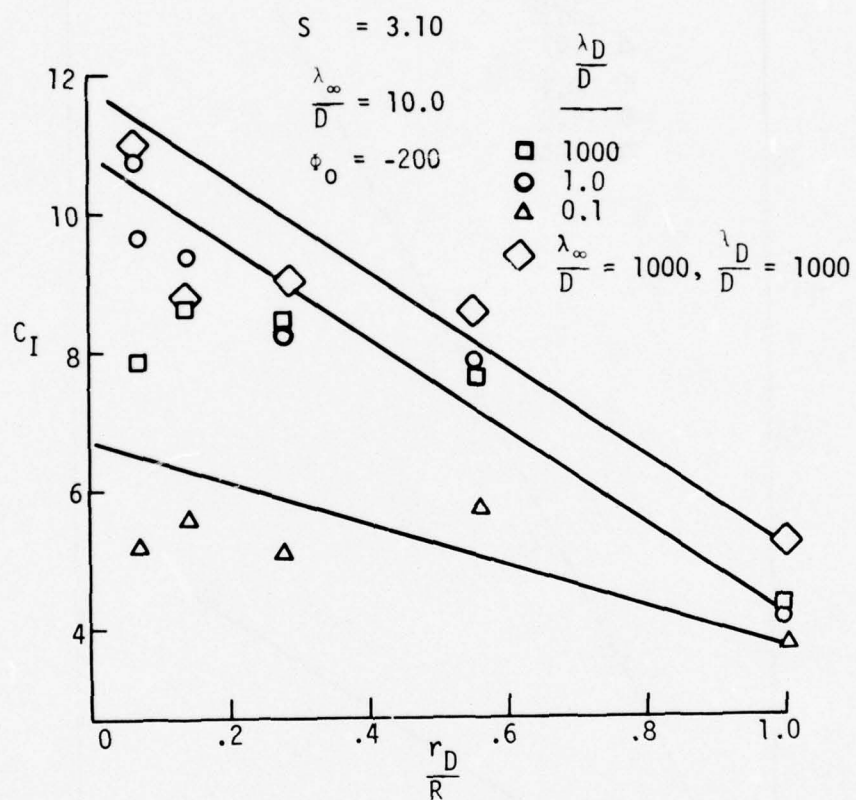ION FLUX VARIATION ACROSS FRONT FACE FOR
NEAR FREE MOLECULE FLOW

$S = 3.10$

$\frac{\lambda_\infty}{D} = 10.0$

$\phi_0 = -200$

$\frac{\lambda_D}{D}$

□ 1000
○ 1.0
△ 0.1

◇ $\frac{\lambda_\infty}{D} = 1000, \frac{\lambda_D}{D} = 1000$

C_I

FIGURE 6

10

of practical concern. The range of the potential from zero to -200 is probably insufficient; but, if the linear relationship does exist between C_I and ϕ_0 for all other parameters fixed, the parametric study for the collisionless limit is complete. This information can now be used to predict the ion flux coefficient C_I for any combination of values of Debye number, λ_D/D, speed ratio, S_i, and front face potential, ϕ_0, in free molecule flow. It will be shown later that the free molecule flow result is valid for a Knudsen number as small as $\lambda_\infty/D = 1$ which corresponds to an altitude of approximately 100 km.

2.2 NEAR FREE MOLECULE FLOW

The ion flux distribution with radius for a Knudsen number of 1.0 is shown in Figure 7. By comparing these results with those for a Knudsen number of 10, it can be seen that the effect of collisions has reduced the ion flux by approximately one-third. Again for large Debye numbers the flux variation across the plate is about a factor of 2, whereas for the small Debye numbers, e.g., $\lambda_D/D = 0.05$, the flux is approximately constant with radius. This indicates that the sheath is very close to the body surface for small Debye numbers and the electric field is approximately constant.

2.3 TRANSITION FLOW (90 KM)

The density variation for both ions and neutrals for a Knudsen number of 0.20 is shown in Figure 8 for Debye numbers 0.02 and 1000. It is seen that there is a considerable separation between the ions and neutrals in contrast to the result at 70 km discussed later. There is also no indication of a gasdynamic shock in the neutral particles which is expected in the continuum case.

Figure 9 shows the flux variation across the front face, where again the stagnation point flux is determined by extrapolation. In extrapolating by eye, the values near the stagnation have less weight because of the smaller number of samples at these interior points. Similar to other Knudsen numbers, the flux becomes uniform as the Debye number decreases.

The variation of the electric potential along the stagnation line is shown in Figure 10. It is seen that for Debye numbers greater than 0.5 the potential distribution does not change and is given by the Laplace solution. For smaller Debye numbers, the potential decreases faster and the sheath becomes smaller. For a Debye number of 0.02, the potential becomes positive at approximately $X/\lambda_\infty = 2.5$.

11

ION FLUX DISTRIBUTION ALONG FRONT FACE FOR
KNUDSEN NUMBER 1.0

FIGURE 7

12
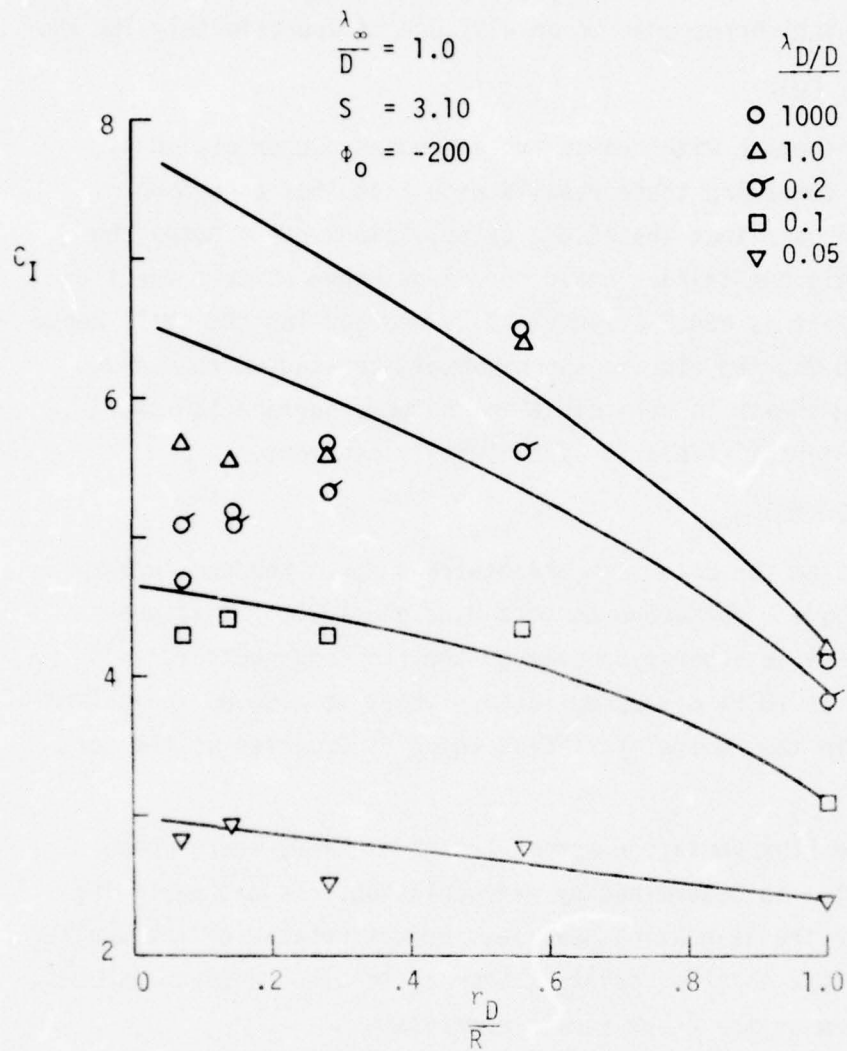
DENSITY DISTRIBUTION ALONG STAGNATION LINE FOR 90 km

$\frac{\lambda_\infty}{D} = 0.20$

$S = 3.1$

$\phi_0 = -200$

• NEUTRAL DENSITY

$\frac{\lambda_D/D}{}$

○ 1000   ION DENSITIES

▽ 0.02

$\frac{X}{\lambda_\infty}$

$\frac{n}{n_\infty}$

FIGURE 8

13

ION FLUX DISTRIBUTION ALONG FRONT FACE AT 90 km

FIGURE 9

14

ELECTRIC POTENTIAL ALONG STAGNATION LINE

FIGURE 10

2.4 NEAR CONTINUUM FLOW (70 KM)

Figure 11 shows the density distributions along the stagnation line for both ions and neutral particles for two extreme values of the Debye numbers, 0.03 and 1000, for a Knudsen number of $\lambda_\infty/D = 0.007$. It should be emphasized that the abscissa is measured in mean free path units X/λ_∞ so that a value of $X/\lambda_\infty = 20$ is in terms of the diameter

$$X/D = (X/\lambda_\infty)(\lambda_\infty/D) = (20)(0.007) = 0.14$$

It is seen from Figure 11 that the first effects of the body on the neutral gas particles occurs at approximately $X/\lambda_\infty \stackrel{\sim}{-} 20$ or $X \stackrel{\sim}{-} 0.14D$.

In Figure 12 the potential field variation along the stagnation line are shown for the two Debye numbers. It is seen that in both cases the electric field penetrates far upstream to accelerate the positive ions toward the collecting plate. The ions are, thus, affected far upstream of the neutral particle gasdynamic shock identified by the rise in density from $X/\lambda_\infty \stackrel{\sim}{-} 20$ to $X/\lambda_\infty \stackrel{\sim}{-} 10$. In Figure 12, large differences in electric potential are shown for Debye numbers of 0.03 and 1000. The linear behavior of the potential for $\lambda_D/D = 1000$ is because the upstream boundary is located at approximately $X/\lambda_\infty \stackrel{\sim}{-} 60$ which corresponds to $X \stackrel{\sim}{-} 0.42D$. For this case, the solution of the Poisson equation is the Laplace solution along the stagnation line determined for a configuration similar to the field between two parallel plates which gives a linear variation. Although the ion density is higher near the body for the larger Debye number the electric field is lower and the net effect on the ion flux at the stagnation point is that it remains approximately constant, $C_I \stackrel{\sim}{-} 2.7$, for the Debye number range; $0.03 \stackrel{\sim}{-} \lambda_D/D \stackrel{\sim}{-} 1000$.

In Figure 13 the ion flux variation across the front face shows two effects. First, the variation with Debye number in the range $0.03 \stackrel{\sim}{-} \lambda_D/D \stackrel{\sim}{-} 1000$ is very small, and the flux at the stagnation is approximately constant. This result is shown later in Figure 15. Secondly, the ion flux peaks sharply at the stagnation point reflecting the very high densities for this near-continuum flow field.

Figure 14 shows velocity field along the stagnation line for both ions and neutrals. Again, as with the density, the effect of the electric field upstream of the disturbance in tne neutral molecules is apparent, the field

16

ION NUMBER DENSITY ALONG STAGNATION LINE

$\dfrac{\lambda_D/D}{}$

● 1000

○ 0.03

$\dfrac{\lambda_\infty}{D} = .007 \quad \Phi_o = -200$

$S = 3.1$

— — — NEUTRAL MOLECULES

$\dfrac{X}{\lambda_\infty}$

$\dfrac{n}{n_\infty}$

10

8

6

4

2

0

0   10   20   30   40   50   60
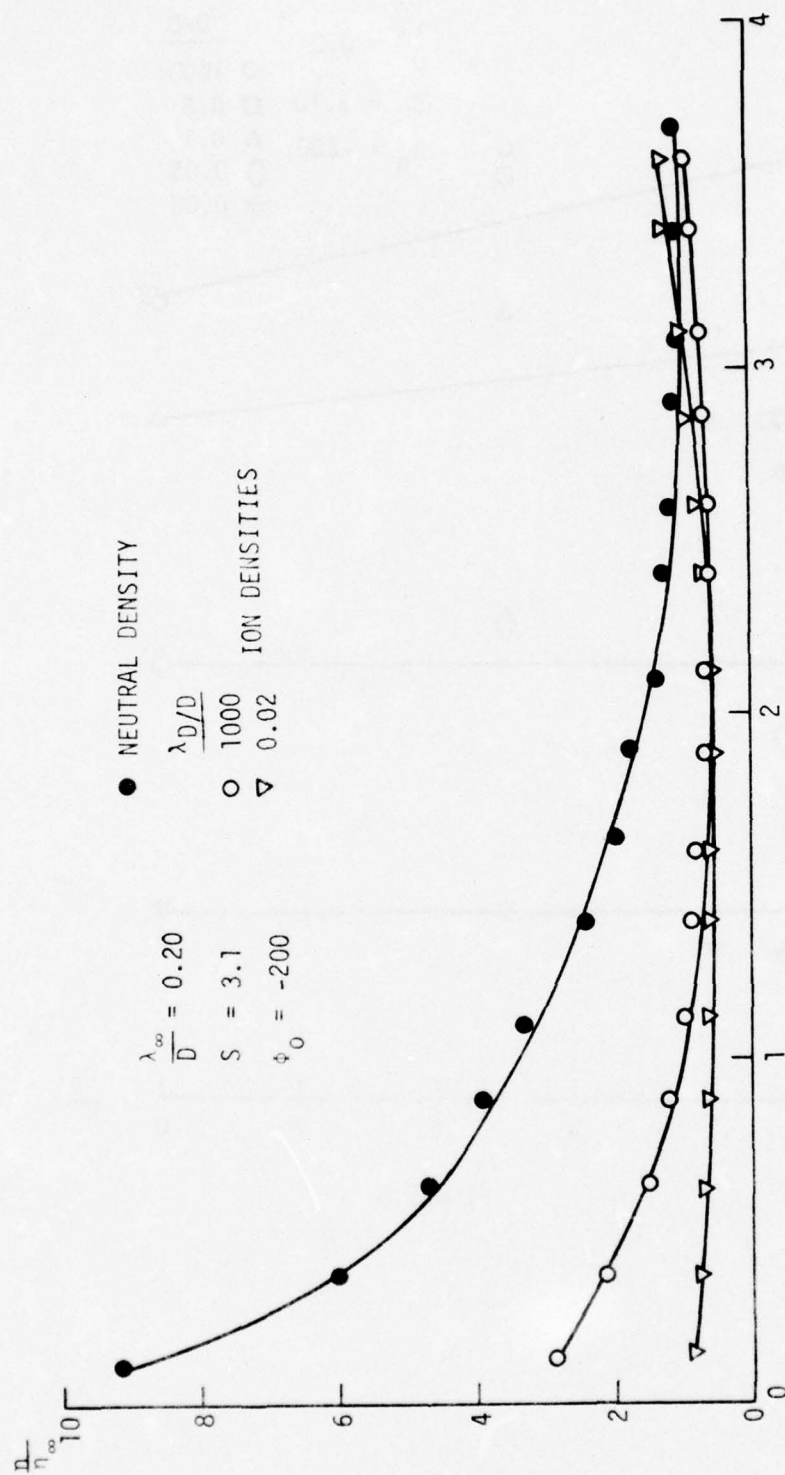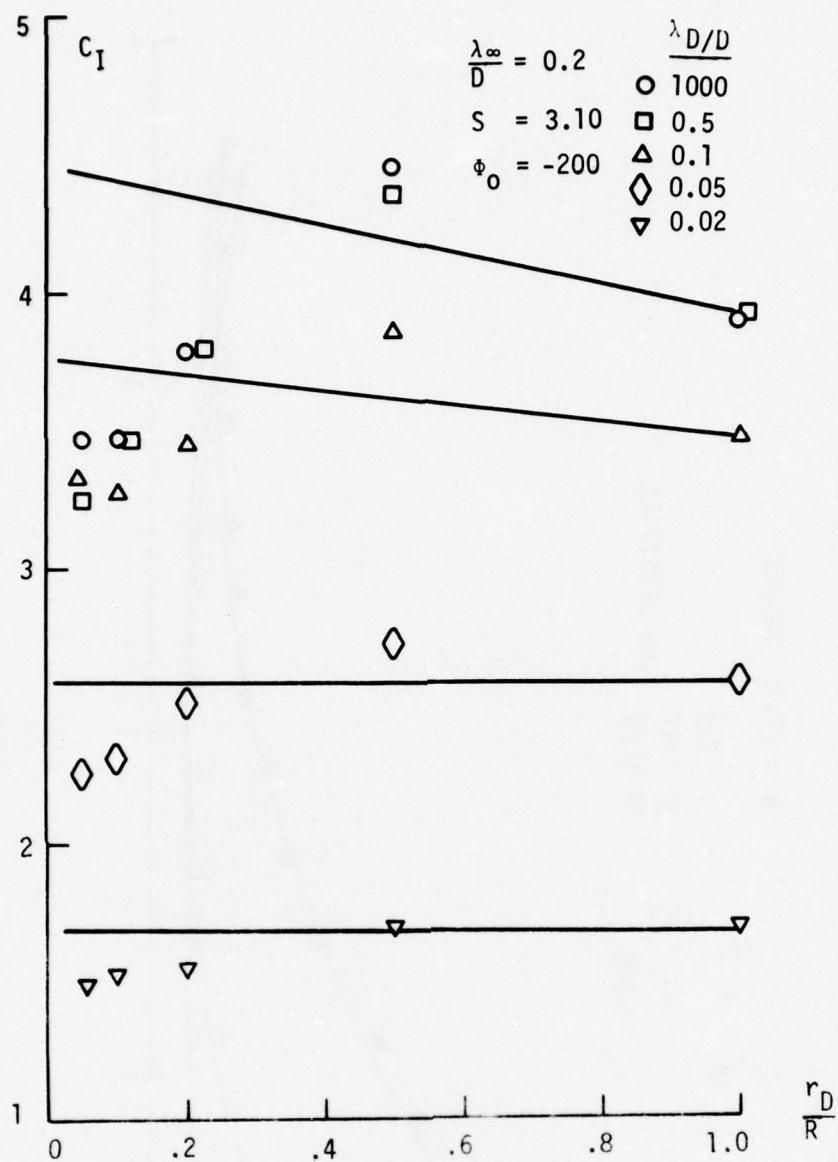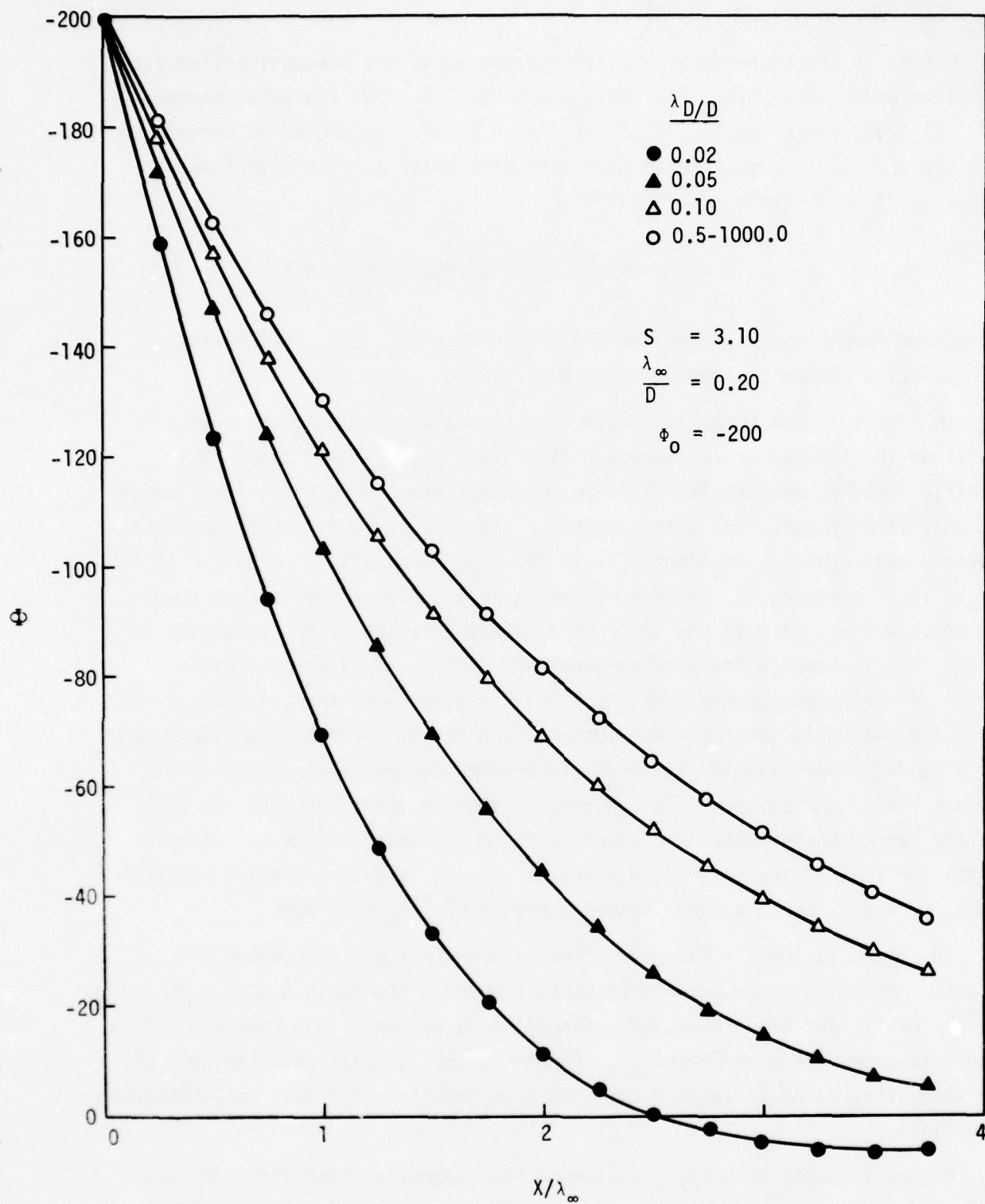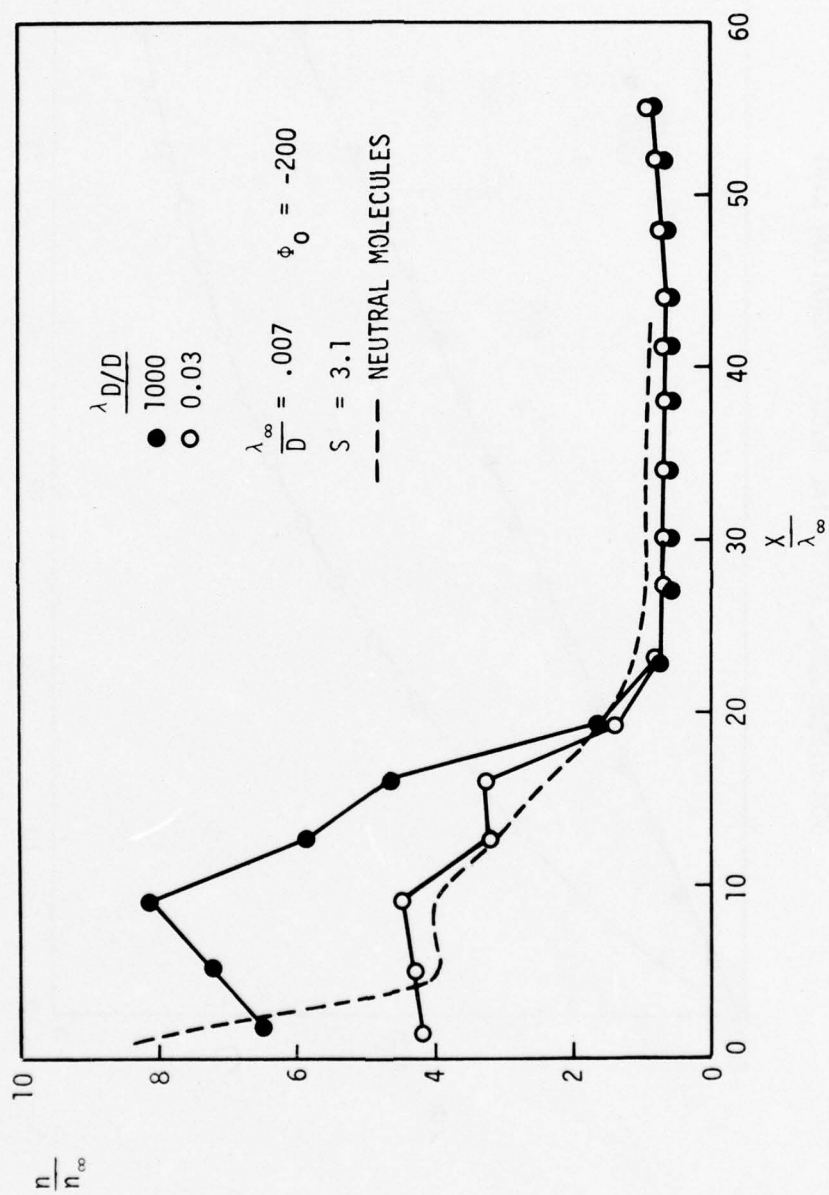
FIGURE 11

17

NON-DIMENSIONAL POTENTIAL ALONG STAGNATION LINE

FIGURE 12

18
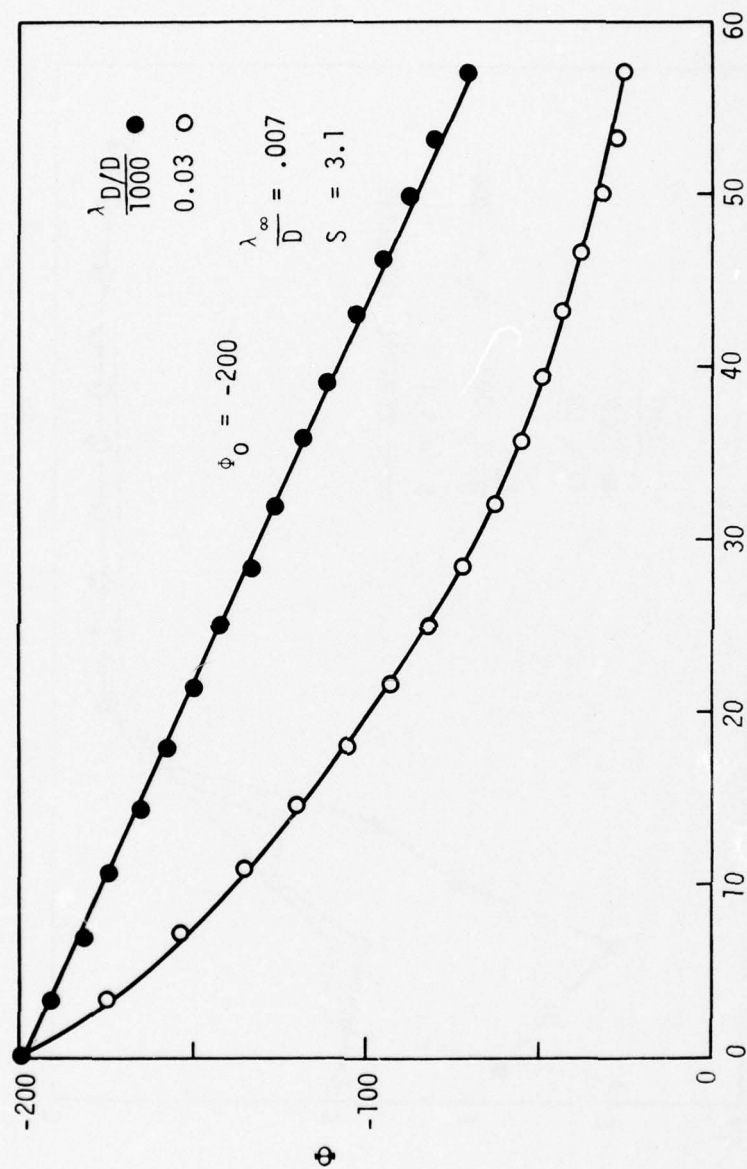
ION FLUX DISTRIBUTION ALONG FRONT FACE AT 70km

FIGURE 13

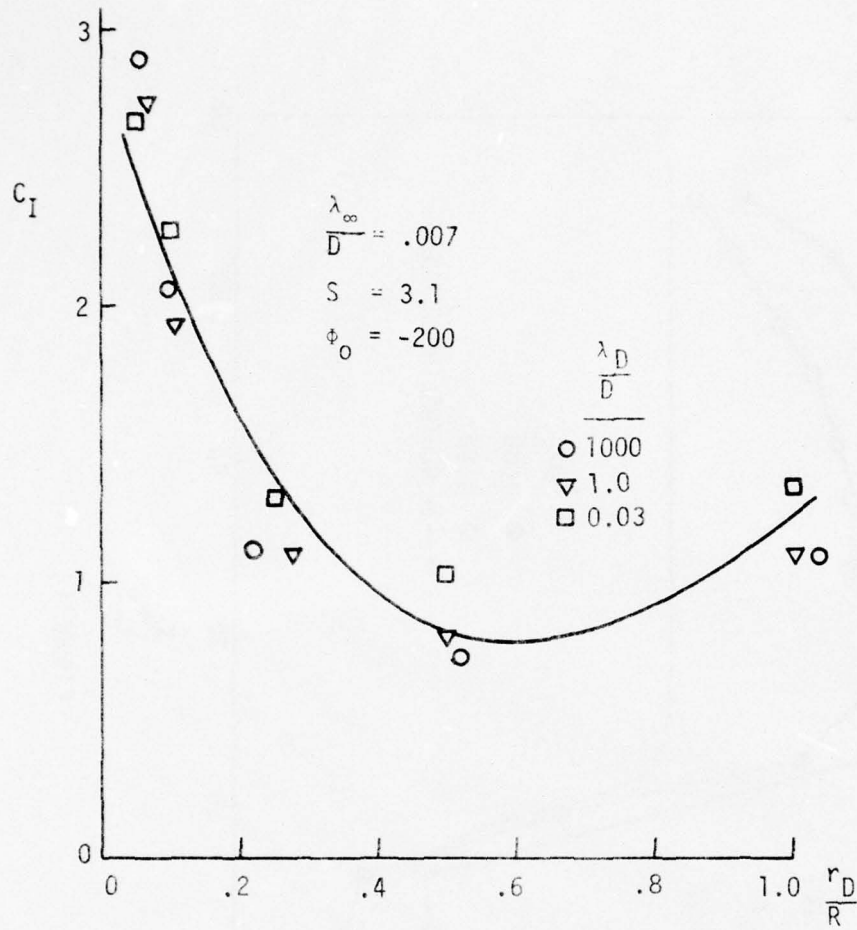ION VELOCITY ALONG STAGNATION LINE

$\frac{\lambda_\infty}{D} = .007$

$S = 3.1$

$\Phi_0 = -200$

$\frac{\lambda_D/_D}{1000}$

● 0.03

○ 0.03

-- NEUTRAL MOLECULES
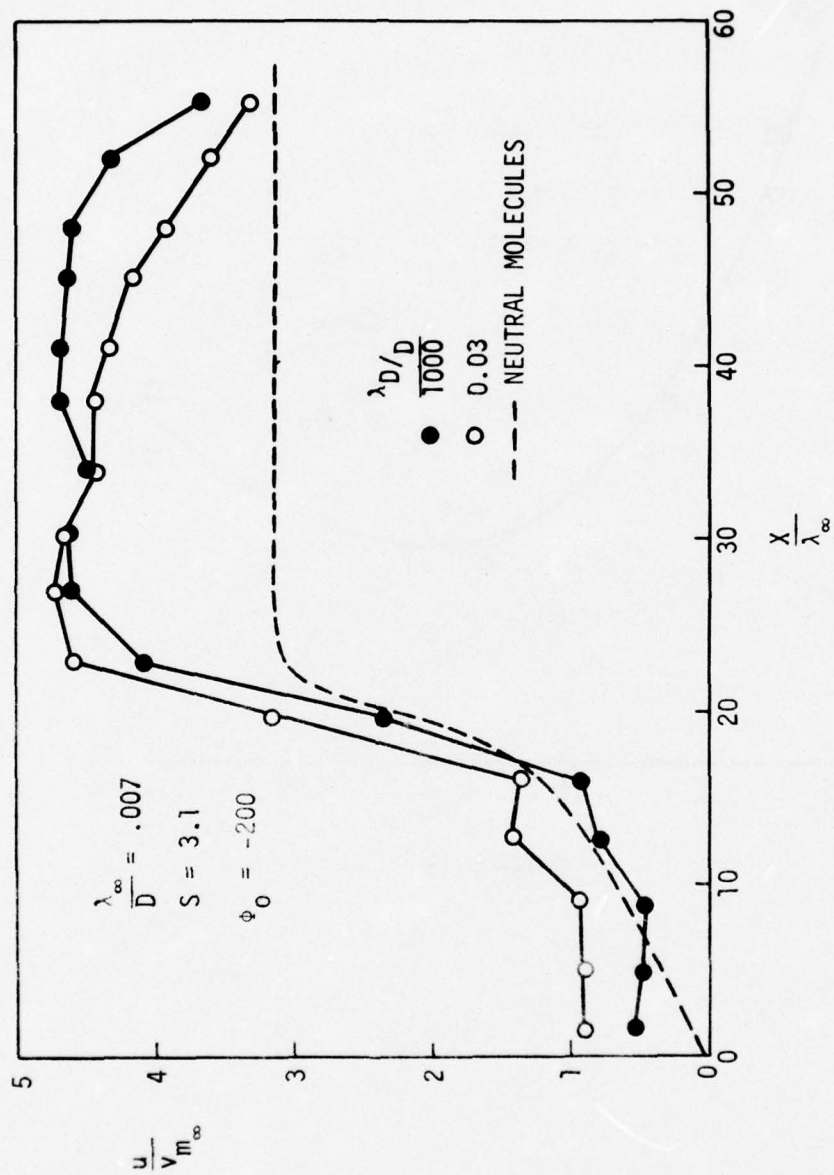
$\frac{u}{v_m\infty}$

$\frac{X}{\lambda_\infty}$

FIGURE 14

corresponding to the larger Debye number again penetrating further from the body. It should be pointed out that the ion velocity at the body surface $(X/\lambda_\infty = 0)$ is not zero, unlike the velocity for the neutrals, since the ions are assumed to be converted to neutrals when they strike the body. These calculations at 70 km required approximately 25 minutes on the CDC 6600 computer for the most time consuming calculations at small Debye number. The ion flux samples for a typical case at small Debye number were about 400 for the stagnation point and 4000 over the entire front face.

2.5 SUMMARY

A summary of the results for the parametric study is shown in Figure 15, where the stagnation ion flux coefficient is shown as a function of Debye number for Knudsen numbers equal to $\lambda_\infty/D = 0.007$, 0.20, 1.0, 10., 1000, a speed ratio of 3.10, and a nondimensional front face potential of -200. Also included on this figure on the left hand side are the computed values of the flux coefficient in the zero-field limit ($\phi_0 = 0$), which represent the minimum value for a given Knudsen number. Note that the value of the zero-field limit for the free molecule case $(\lambda_\infty/D = \infty)$ is unity as required.

It can be seen that the variation of the flux coefficient C_I with Debye number exhibits a common trend for Knudsen numbers $\stackrel{>}{-} 0.20$. That is the flux coefficient is constant as the Debye number is reduced until a "break-point" is reached, after which the flux coefficient decreases with decreasing Debye number. A further observation is that the break-point occurs at a Debye number approximately equal to the Knudsen number for transitional flows; e.g. $\lambda_\infty/D = 0.20$. For the collisionless flow $\lambda_\infty/D \stackrel{>}{-} 10$, the break point occurs at a value of $\lambda_D/D \stackrel{\sim}{=} 0.5$ or $\lambda_D \sim$ body radius. The effects of collisions can be seen in the results for Knudsen number unity, e.g. the reduction in the flux coefficient below the collisionless limit. However, the "break-point" remains at approximately 0.5. The results for the near-continuum flow with Knudsen number 0.007 exhibit no "break-point" for the range of Debye numbers considered. If the "break-point" is assumed to occur at a Debye number approximately equal to the Knudsen number the transition should occur at a Debye number near 0.007. Calculations for Debye numbers less than 0.03 for these conditions have not been successful to date because of numerical instabilities.

21

STAGNATION POINT FLUX WITH DEBYE NUMBER

FIGURE 15

22
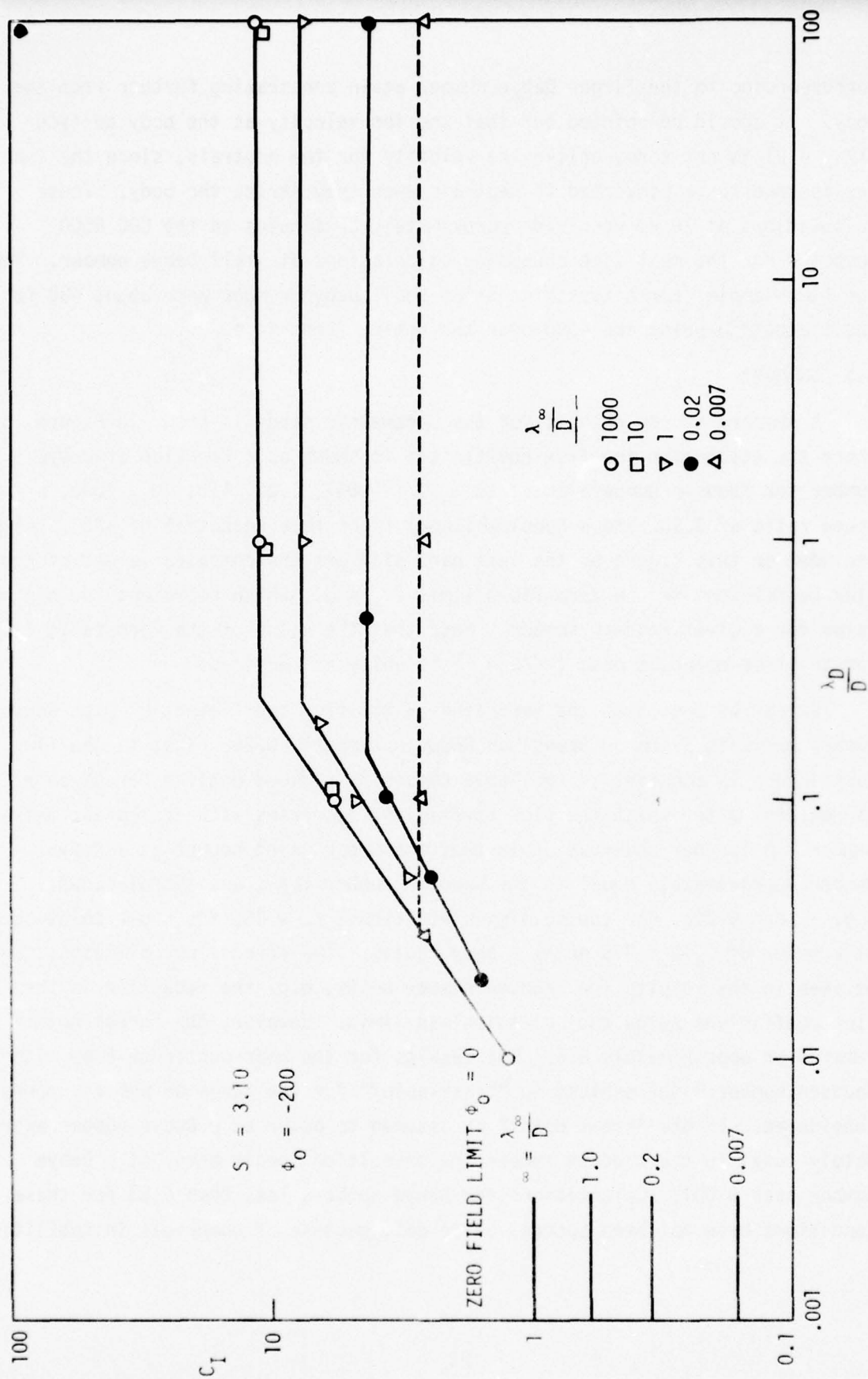
Although these results do not represent a complete parametric study the following trends seem reasonable.

1) The flux coefficient decreases with decreasing Debye number for a fixed Knudsen number.

2) The flux coefficient decreases with decreasing Knudsen numbers for fixed Debye numbers greater than the body radius, i.e. $\lambda_D/D > 0.5$.

3) The "break point" for the variation of the ion flux coefficient with Debye number can be estimated by

$$(\lambda_D)_{BP} = \text{minimum} (\lambda_\infty, R)$$

i.e. the "break point" is given by $(\lambda_D)_{BP} = \lambda_\infty$ or $(\lambda_D)_{BP} = R$ whichever is less. Therefore, for $\lambda_D > (\lambda_D)_{BP}$ the ion flux is determined by taking $\lambda_D \rightarrow \infty$.

These limits for the "break point" are shown on Figure 2. It can be seen that in the "range of interest" below 90 km the ion flux can be determined by the infinite Debye number limit.

In many applications the quality of the flux entering the instrument is just as important as the number of particles. Figure 16 gives the percentage of free stream ions in the stagnation point flux as a function of Knudsen number. These results are approximately independent of Debye number for the range $0.01 \lesssim \lambda_D/D \lesssim 1000$. This shows, for example, that below an altitude of 90 km ($\lambda_\infty/D = 0.2$) the entire flux has been affected by the body and only for Knudsen numbers greater than 10 is the flux completely undisturbed.

Figure 17, which is reproduced from Sugimura and Vogenitz (1975) shows the variation of the stagnation point flux for the zero field limit ($\phi_0 = 0$) as a function of Knudsen number or altitude. At an altitude of 70 km ($\lambda_\infty/D = 0.007$) this ion flux coefficient is approximately

$$C_I \simeq 0.17$$

Sonin (1967) gives a continuum prediction for the zero field limit

$$C_I \simeq 2 \frac{\rho_0}{\rho_\infty} \frac{1}{\sqrt{\pi \, S_c R_e}}$$

23

FRACTION OF FREESTREAM IONS IN STAGNATION POINT FLUX

% OF THE TOTAL STAGNATION POINT ION FLUX DUE TO FREESTREAM IONS

$S = 3.10$

$\Phi_0 = -200$

$0.01 \leq \dfrac{\lambda_D}{D} \leq \infty$

$\dfrac{\lambda_\infty}{D}$
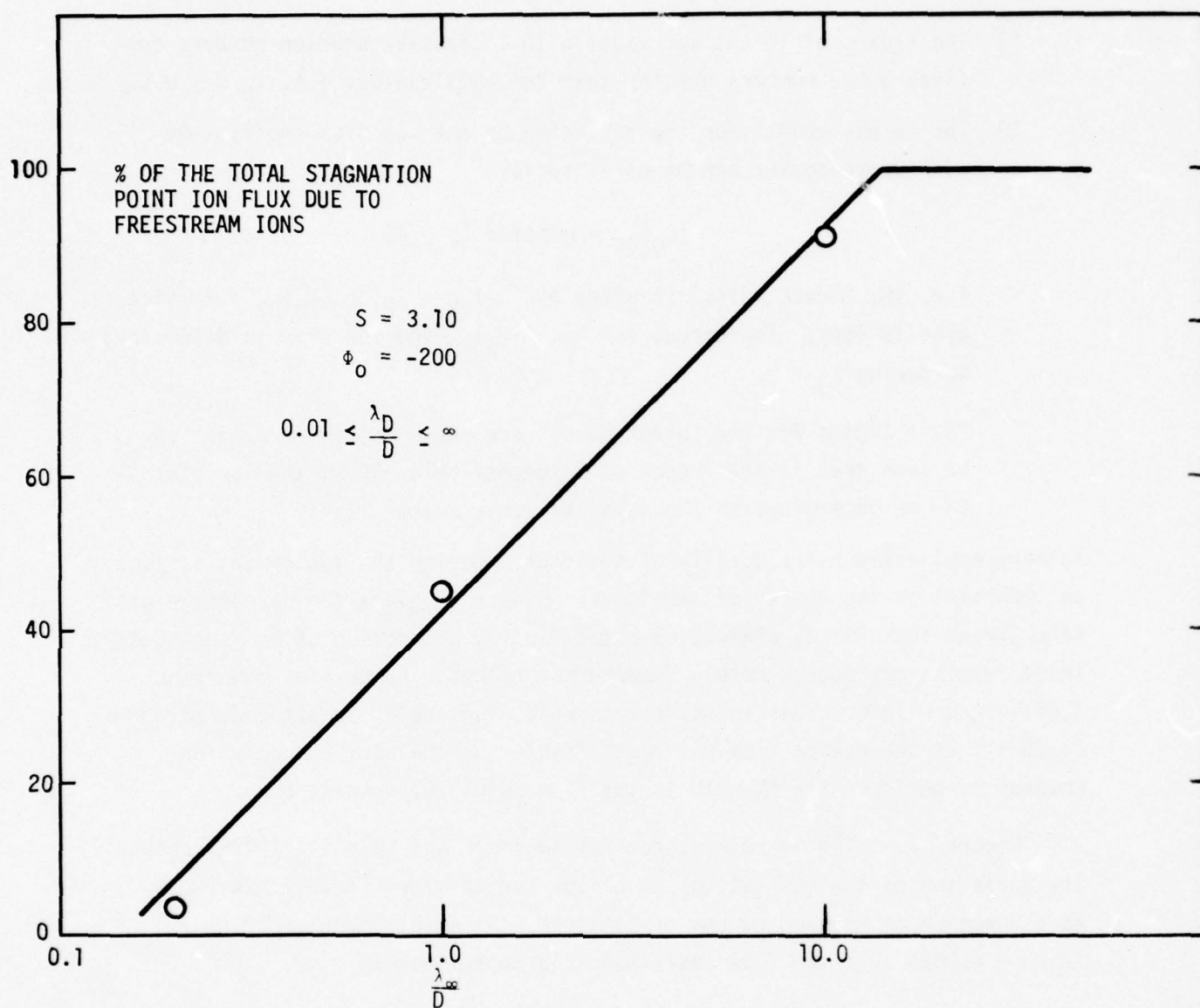
FIGURE 16

where   Sc = Schmidt number = $\dfrac{\mu_o}{\rho_o D_o}$

R_e = Reynolds number = $\dfrac{\rho_o U_\infty R}{\mu_o}$

ρ_o = Stagnation density

ρ_∞ = Free Stream density

The diffusion coefficient can be estimated by the simple relation given by Jeans (1940).

$$D_o \simeq 1/3 \sqrt{\frac{2kT}{m}}\, \lambda$$

If the stagnation conditions are taken to be the conditions behind a normal shock for a gas with a ratio of specific heats equal to 1.4 the value of the flux coefficient becomes

$$C_I \simeq 0.16$$

which compares favorably with the Monte Carlo results. However, if the velocity and temperature are fixed the variation of the flux coefficient with mean free path from Sonin's result becomes

$$C_I \sim \sqrt{\lambda}$$

This variation shown in Figure 17 appears reasonable for lower altitudes but cannot be extended to much higher altitudes. A more detailed investigation is required to determine the correlation between the continum prediction and the Monte Carlo results. Also shown on Figure 17 is the quality of the flux for the zero field case. Here the flux at 90km is found to be composed entirely of ions which have suffered collisions with neutral molecules. It should be noted here that the collision cross sections for ion-neutral and neutral-neutral encounters were taken to be equal. The effects of different cross sections are discussed by Sugimura and Vogenitz (1975).

25

STAGNATION POINT ION FLUX VARIATION WITH KNUDSEN NUMBER FOR ZERO PLATE POTENTIAL

$S = 3.1$
$\Phi_0 = 0$

SYMBOL

○ TYPE (I) FLUX; FREESTREAM IONS

△ TYPE (III) FLUX; IONS WHICH HAVE COLLIDED
WITH NEUTRALS WHICH HAVE COLLIDED WITH THE
BODY OR OTHER TYPE (III) NEUTRALS

□ TOTAL FLUX = I + III

— — — CONTINUUM, SONIN (1967)

C_r

λ_∞/D

(70 KM)   (90 KM)   (95 KM)   (110 KM)   (120 KM)

0.001   0.01   0.10   1.00   10.0   100

FIGURE 17

26
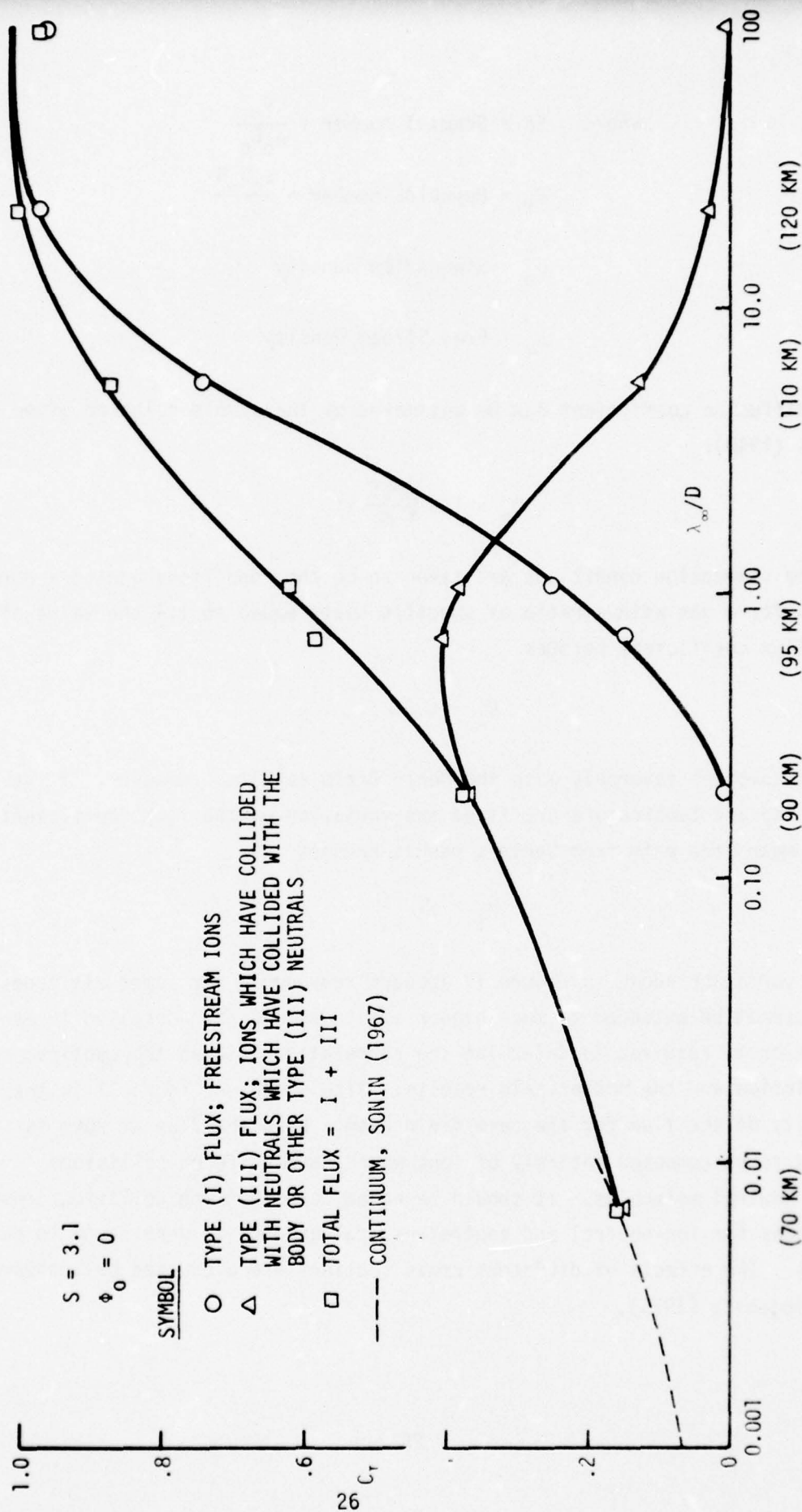
From the results of the parametric study, a functional relation of the form

$$C_I = f(S_\infty, \phi_0, \lambda_\infty/D, \lambda_D/D)$$

can be determined for the altitudes which are characterized by Knudsen numbers in the transitional regime or larger, $\lambda_\infty/D = 0.20$ to ∞ in the present study. For Knudsen numbers less than transitional the results shown in Figure 15 indicate that the correlational function will be complicated by the location of the "break point." This problem becomes unimportant, however, if the range of parameters is restricted to the "range of interest" shown in Figure 2.

Furthermore, in the collection of large positive (or negative) ions the number of collisions that the ions experience before entering the mass spectrometer is important because of perturbations to the ambient states, i.e., chemical, internal, etc. The result indicated here that the fraction of free stream ions is independent of the Debye number and electric field may be of some use to instrument designers.

3. SIDEWALL POTENTIAL EFFECTS

In the Monte Carlo results reported previously the space charge effects on the electric potential of the sidewall were neglected. That is the boundary condition for the potential on the vehicle side walls was assumed to be zero. However, it is known that typical values of floating potentials are 1 to 3 volts negative. In order to investigate the effects of finite space charge on the sidewall the boundary conditions for the potential were modified in the following way.
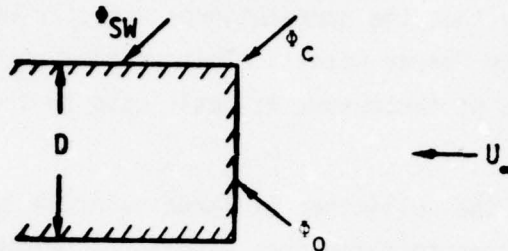
The applied front face potential, ϕ_0, in a non-dimensional form is:

$$\Phi_0 = \frac{e\phi_0}{kT_\infty} = 11,600 \frac{\phi_0 (\text{volts})}{T_\infty (°K)}$$

The non-dimensional sidewall potential is:

$$\Phi_{SW} = 11,600 \frac{\phi_{SW}}{T_\infty}$$

and the potential at the corner of the vehicle is defined as:

$$\phi_C \equiv \frac{1}{2} (\Phi_0 + \Phi_{SW})$$

Recall that in the introduction the systematic parameter study was to be made for a fixed non-dimensional potential of

$$\Phi_0 = -200$$

Therefore, in the absence of a sidewall potential the ambient temperature does not enter into the analysis. When the space charge effect on the vehicle is included by assuming a fixed sidewall voltage, e.g., $\phi_{SW} = -1$ volt, the ambient temperature becomes a parameter. If a value of $\phi_{SW} = -1$ volt is assumed the following results are obtained:

Altitude(km)	T(°K)	$\Phi_{SW} = 11,600 \dfrac{\phi_{SW}}{T_\infty}$
70	216	-53.7
90	184	-63.0
110	257	-45.2
130	534	-21.7

This table shows that the minimum temperature occurs at 90 km and gives the maximum sidewall potential.

One of the reasons for examining the effects of the sidewall potential buildup was that the solution of Poisson's equation for the electric potential became unstable for small Debye lengths. This difficulty was caused by large changes in the electric potential over distances comparable to the Debye length especially at the corner of the vehicle for the usual boundary conditions:

$$\Phi_o = -200$$

$$\Phi_{SW} = 0$$

$$\Phi_C = -100$$

Therefore, in an attempt to reduce the gradient in the potential along the body, a finite potential was placed on the sidewalls. With this modification in the boundary condition, solutions were obtained at smaller Debye lengths than for the earlier attemps at an altitude of 70 km.

However, when a sidewall potential of 1 volt negative was assumed for the other altitudes results which were inconsistent with previous trends were obtained. For example at the following conditions:

$$S = 3.10$$

$$\frac{\lambda_D}{D} = 1000 \text{ (Laplace solution)}$$

$$\Phi_o = -200$$

$$\Phi_{SW} = 0$$

29

The ion flux at 90 km was found to be greater than at 70 km. If a sidewall voltage of -1 volt is assumed the ion flux at 90 km is less than at 70 km because the non-dimensional sidewall potential is larger at 90 km. Since the objectives of this phase of the study were to obtain general trends in the variation of the parameters it was decided to minimize the number of variables by ignoring the sidewall potential in most of our calculations. In the future if the positive ion flux is to be predicted along a given flight trajectory the front face and sidewall voltages should be fixed and all the non-dimensional potentials ϕ_0, ϕ_C, and ϕ_{SW} should be a function of altitude.

4. ANGLE OF ATTACK EFFECTS

The difficulty in considering angle of attack effects is that the flow symmetry is destroyed and a three dimensional flowfield must be considered. A Monte Carlo simulation code to simulate the flow of neutral molecules about general body shapes at arbitrary angles of attack is currently operational the AFGL computing system. Modifications to this program are necessary before any charged particle calculations can be made. In particular a three-dimensional Poisson equation solution is required to calculate an electric field consistent with the charged particle flowfield.

The geometry for the body at angle of attack is shown in Figure 18. The parameters which characterize the three dimensional effects are the angle of attack, α, and the azimuthal angle, θ. In the two dimensional case $\alpha = 0$ and there are no variations with θ.

Figure 19 shows the density distribution of neutral molecules in a plane parallel to the front face as a function of the azimuthal angle for three values of the angle of attack: $\alpha = 0$, $10°$, and $20°$. This distribution is given for a point located in a plane a distance $0.091R$ downstream of the front face (R is the body radius shown in Figure 18) and a distance $0.62R$ from the vehicle sidewall As expected the density for non zero angles of attack is highest for small θ where the flow is compressed and lowest for $\theta \cong 180°$ where the flow has expanded. The density changes are also greater for higher angles of attack. An interesting coincidence in this case is that the density for all three angles of attack are approximately the same at $\theta \cong 100°$. The value of the density ratio at the stagnation point does not differ by more than 10% as the angle of attack varies from $0°$ to $20°$. Therefore, the flux entering the orifice at the stagnation point is only slightly affected for these flight conditions.

31

COORDINATES FOR THREE DIMENSIONAL FLOWFIELD
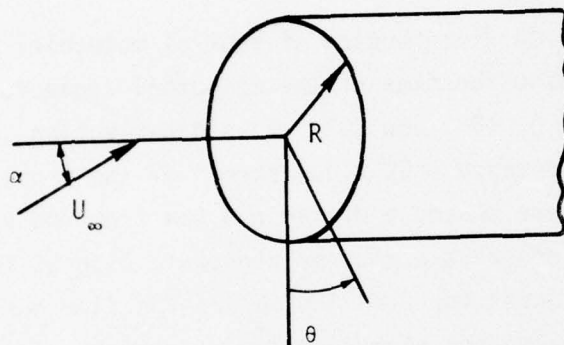
α = ANGLE OF ATTACK

θ = AZIMUTHAL

FIGURE 18

32

AZIMUTHAL VARIATION OF DENSITY

$\dfrac{\lambda_\infty}{D} = .43$

$S = 4.0$

$\bigcirc\ \alpha = 10°$

$\triangle\ \alpha = 20°$

$\dfrac{n}{n_\infty}$

2.0

1.5

1.0

COMPUTED FOR $\alpha = 0$

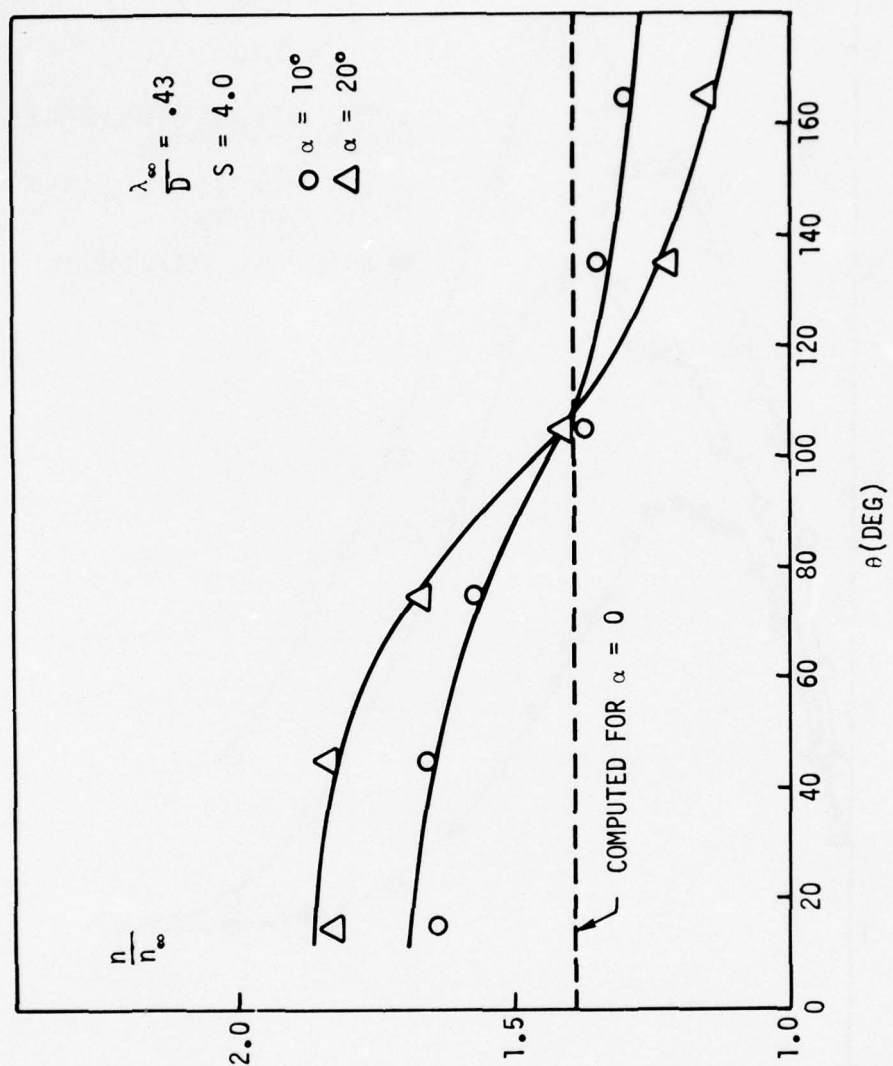0   20   40   60   80   100   120   140   160

θ(DEG)

FIGURE 19
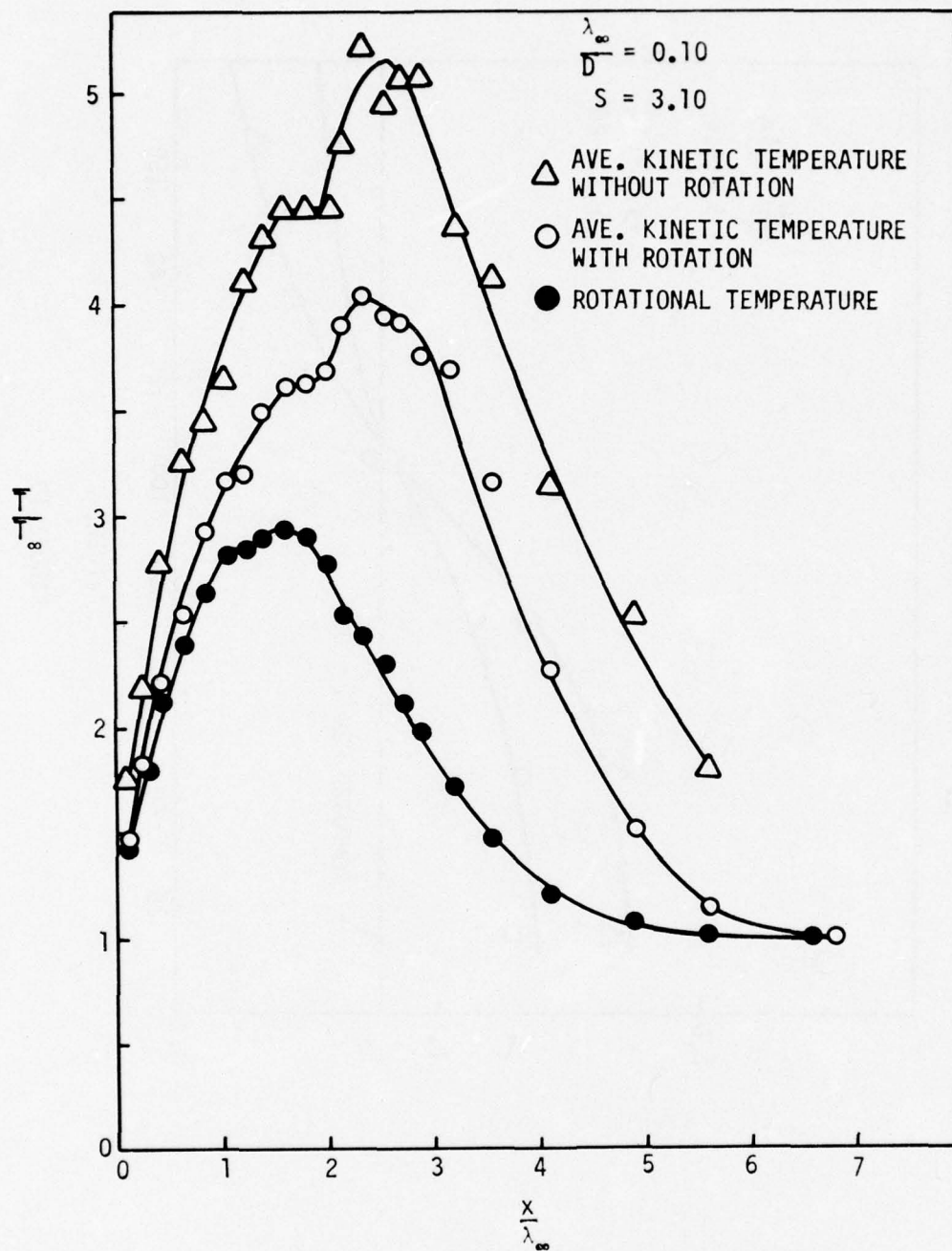
33

TEMPERATURE DISTRIBUTIONS ALONG STAGNATION LINE

FIGURE 20

5. INTERNAL DEGREES OF FREEDOM

All of the results presented were based on a hard sphere molecular model
with no internal degrees of freedom. A more realistic molecular model would
include the effects of rotational and vibrational degrees of freedom. For
example, Figure 20 shows a comparison between the average kinetic or transla-
tional temperature and the rotational temperature along the stagnation line.
This calculation was performed for a neutral gas at a Knudsen number of 0.10
corresponding to an altitude of 88 Km and a speed ratio of 3.10. If the
gas were in thermodynamic equilibrium the two temperatures would be identical.
However, the kinetic temperature is shown to rise very rapidly while the
rotational temperature remains much lower. Finally at a distance of
approximately

$$\frac{x}{\lambda_\infty} \cong 1.0$$

the temperatures are again in equilibrium. A simple explanation of this
effect can be made by noting that rotational equilibrium requires many more
collisions than translational equilibrium, e.g. typically a ratio of 10:1.
The flow is assumed to be in equilibrium far upstream of the body but as
the presence of the body is encountered the density increases. However,
this density rise is not sufficient to maintain equilibrium and the rota-
tional temperature falls below the kinetic temperature. Finally, as the
density increases through the "shock" a level is reached where the collisions
are sufficient to reestablish equilibrium. Also shown in Figure 20 is the
kinetic temperature distribution if the rotational energy is ignored. It
is seen that without the rotational energy which acts as an energy sink the
translational temperature is uniformly higher.

A more explicit example of the effect of molecular collisions is given
in Figure 21 where the stagnation line temperature distribution is presented
for a Knudsen number of 0.007 corresponding to an altitude of 70 Km and a
speed ratio of 3.10. The density increase and the collision frequencies are
much higher than for the results at a Knudsen number of 0.10. The effects
of the increased collisions on the temperature distributions is seen in the
near equilibrium in the two temperatures for $x/\lambda_\infty < 5.0$. Note that the abscissa

35

TEMPERATURE DISTRIBUTIONS ALONG STAGNATION LINE AT 70 km

$\dfrac{\lambda_\infty}{D} = .007$ $S = 3.10$

O AVERAGE KINETIC TEMPERATURE
● ROTATIONAL TEMPERATURE

$\dfrac{T}{T_\infty}$

$\dfrac{X}{\lambda_\infty}$
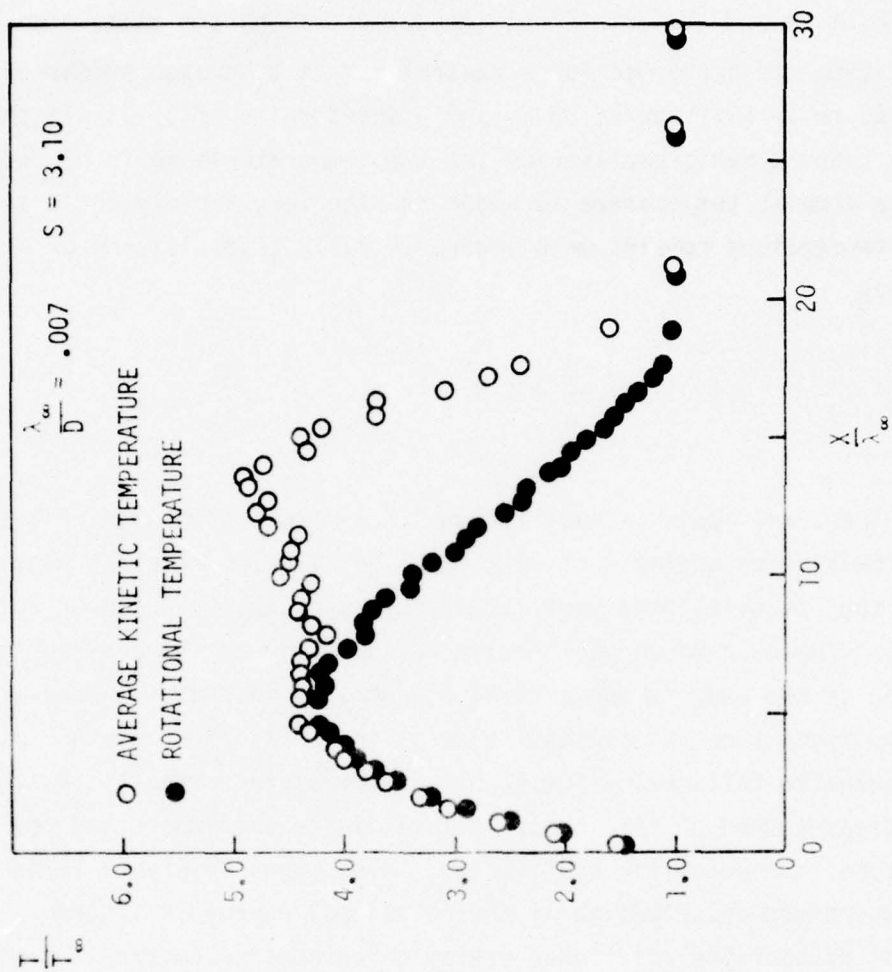
FIGURE 21

in both Figures 20 and 21 is the distance, x, divided by the mean free path, λ_∞, which is approximately 15 times greater at 88 Km.

If the velocity distribution function is examined, the initial equilibrium Boltzmann distributuion far upstream of the body is distorted as the non equilibrium effects are encountered. Again, as the collision frequency increases near the body equilibrium conditions are reestablished.

The effects of rotational non equilibrium on the collected ion flux are not obvious. However, the addition of internal degrees of freedom acts as an energy sink which certainly influences the other flow parameters. From the calculations at Knudsen number 0.10 the stagnation point flux for zero potential ($\psi_0 = 0$) differs by about 10% when rotational energy is included. Further computations are required to determine the extent of this difference due to statistical scatter.

6. CHEMICAL REACTIONS

It has been shown in Section 2 that the properties of the ions collected by the mass spectrometer are distorted from the ambient values. In particular for large highly clustered ions the distortion during sampling may be serious enough to prevent the determination of the true cluster ion distribution. The effects of the change in chemical composition can be assessed in a straightforward way through the direct simulation Monte Carlo method by treating the chemical reactions as collision processes.

A typical bimolecular reaction may be written as

$$A + B \xrightarrow{k(T)} C + D$$
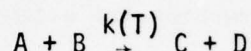
where A, B, C, D represent separate species, e.g. molecules, ions, electrons. If the molecules can be idealized as reactive hard spheres with total elastic scattering cross section, σ_0, the total reaction cross section σ_R is given by

$$\sigma_R(E) = \begin{cases} 0 \text{ for } E < E^* \\ \sigma_0 \left(1 - \frac{E^*}{E}\right) \text{ for } E \geq E^* \end{cases}$$

where E^* = threshold energy

  E = relative energy in the collision

and the reaction rate coefficient, $k(T)$, is found to be

$$k(T) = \sigma_0 \left(\frac{8kT}{\pi\mu}\right)^{1/2} \exp\left(\frac{-E^*}{kT}\right)$$

where μ = reduced mass.

If $k(T)$ and E^* are known for the important processes in the ionosphere, the cross section σ_0 can be determined and fed directly into the Monte Carlo Simulation calculations. This model can be extended to include internal degrees of freedom and deviations from hard sphere interactions. Although no calculations involving chemical reactions has been attempted for the ion collection processes the model has been used successfully to predict radiation effects in high altitude plumes.

7. NEGATIVE ION COLLECTION

The assumptions and the complete formulation of the Monte Carlo simulation are detailed in Vogenitz (1973). Most important of the assumptions regards the treatment of the electrons. For the positive ion collection, the front face is negatively charged which repels the electrons and attracts the positive ions. The negative front face potential was assumed large enough so that the electrons could be taken to be in equilibrium with the local potential and determined by the Boltzmann distribution.

$$\frac{N_e}{N_{e_\infty}} = \exp(e\phi/k\, T_e)$$

where

N_e = electron number density

N_{e_∞} = free stream value

ϕ = electric potential

T_e = electron temperature

e = charge on electron

This assumption was shown to be accurate and was then used throughout the previous studies. The great simplification of this assumption was that the electron trajectories could be ignored and only the ion motion was computed with the only coupling between the ion and electron distributions occurring through the electric potential determined from Poisson's equation

$$\nabla^2 \phi = \left(\frac{\lambda_\infty}{\lambda_D}\right)^2 (\overline{N}_i^+ - \overline{N}_e)$$

where

$\phi = \dfrac{e\phi}{kT_\infty}$ = non-dimensional electric potential

λ_∞ = mean free path

λ_D = Debye length

$\overline{N}_i^+ = \dfrac{N_i^+}{N_{i_\infty}}$ = positive ion number density ratio

$\overline{N}_e = \dfrac{N_e}{N_{e_\infty}}$ = electron number density ratio

39

The collection of negative ions requires a positive collecting potential on the front face which, however, also attracts the electrons which will reduce the collecting potential and the effectiveness of the instrument. The sampling of negative ions requires a circular double disk configuration; Sherman and Parker (1970), on the front face to repel the electrons while still collecting negative ions. The geometry and the potential distribution along the front face of the instrument payload will be approximated as shown in Figure 22. Although the face potential, Φo, would be greater than the mask potential, Φe, the mask has greater area. The radii r_o and r_e define the disks corresponding to the two potentials. Therefore, only the proper ratio of ϕ_o to ϕ_e will allow the ions to pass through the collecting orifice for a given set of free stream and boundary conditions. The electron motion in this case cannot be ignored, and the equilibrium assumption for the electrons is no longer valid. This is the major complication introduced by the negative ion collection which was not encountered in the sampling of positive ions.

These complications can be seen by comparing the electron and ion velocities. The thermal velocities for the electrons and ions are given by

$$\overline{V}_i = \sqrt{2 \frac{k}{m_i} T_i} \qquad \text{for ions}$$

$$\overline{V}e = \sqrt{2 \frac{k}{m_e} T_e} \qquad \text{for electrons}$$

where
T_i, T_e = ion and electron temperatures
m_i, m_e = ion and electron masses

40
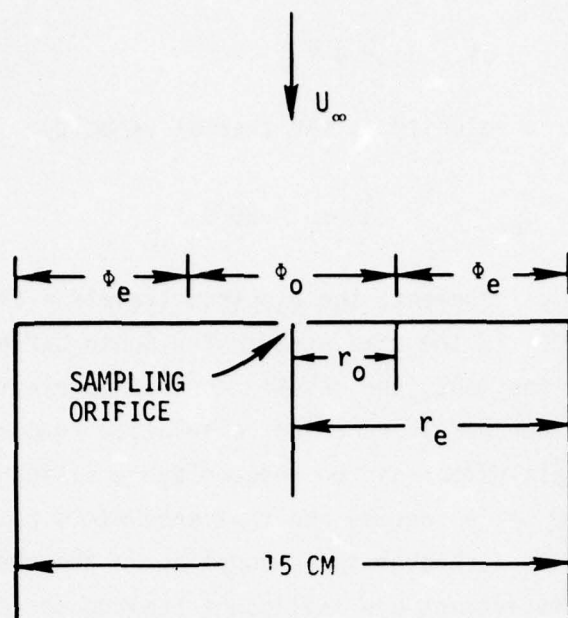
ϕ_c = positive collection potential for negative ion

ϕ_e = negative electron mask potential

Figure 22. Front Face Geometry

The ratio of these speeds are given by

$$\frac{\overline{V}_e}{\overline{V}_i} = \sqrt{\frac{m_i}{m_e}}\sqrt{\frac{T_e}{T_i}}$$

which for equal temperatures, $T_i = T_e$, and an ion molecular weight of 30 becomes

$$\frac{V_e}{V_i} = 235$$

Since the vehicle or free stream velocity, U_∞, is roughly 3 to 5 times the ion thermal speed, the ions are characterized by the free stream velocity

41

$$U_i \simeq U_\infty \simeq 4 \, \overline{V}_i$$

whereas the typical electron velocity is the thermal velocity

$$U_e \simeq V_e \simeq 235 \, V_i \simeq 60 \, U_\infty$$

Therefore, for a given time increment, the electron travels a distance 60 times the ion displacement. If the time step in the Monte Carlo calculations is given by Δt_i for the ions, the result requires 60 electron time steps to equal Δt_i. In other words, each ion calculation requires 60 electron calculations. This number can be reduced by recalling that both the electrons and ions are trace species and that encounters between charged particles are neglected except through their coupling in the electric potential. The only direct interactions are collisions between the charged particles and the neutral molecules which can be characterized by the mean free paths

$$\lambda_{en} = \frac{1}{\sqrt{2} \, Q_{en} \, N_n} \qquad \text{for electrons/neutrals}$$

$$\lambda_{in} = \frac{1}{\sqrt{2} \, Q_{in} \, N_n} \qquad \text{for ions/neutrals}$$

where $\qquad\qquad N_n$ = number density of neutrals

$Q_{en}, \, Q_{in}$ = collision cross sections

Assuming hard spheres, the collision cross sections for two different particles is given by

$$Q_{12} = \pi \left(\frac{\sigma_1 + \sigma_2}{2} \right)^2$$

where $\qquad\qquad \sigma_1, \, \sigma_2$ = particle diameters

42

For the ions, $\sigma_i \simeq \sigma_n$ and $Q_{in} \simeq \pi \sigma_n^2$, but for the electrons $\sigma_e \ll \sigma_n$ and $Q_{en} \simeq \pi \sigma_n^2/4$ The ratio of mean free paths is then given by

$$\frac{\lambda_{en}}{\lambda_{in}} = \frac{Q_{in}}{Q_{en}} \simeq 4$$

Therefore, if an ion travels a distance λ_{in} in time increment Δt_i an electron displacement can be $\lambda_{en} \sim 4 \lambda_{in}$. This reduces the number of electron time steps to equal Δt_i from 60 to 60/4 = 15. In rough terms, this means that the negative ion collection calculations will take approximately 15 times as long as the equivalent positive ion calculation which ignored the electron trajectories.

A procedure to be used in the negative ion sampling involving a complex iteration procedure has been formulated and is being implemented. However, preliminary results for the limiting case of free molecule flow and large Debye number are presented along with calculations for electron trajectories.

7.1 FREE MOLECULE FLOW AND INFINITE DEBYE NUMBER

In the limit of very large Knudsen and Debye numbers the collection of negative ions can be predicted with the same computer code used for the positive ion calculations. For large Debye numbers the electric field is not affected by the ion-electron distribution and the potential is given by the Laplace solution. This case is not insignificant since it was found in Section 2 that the Laplace solution was valid for Debye numbers as small as 1.0. Although the validity of the Laplace solution must be determined again for the negative ion processes it should be valid for a similar range of Debye numbers. The geometrical configuration for the collection of negative ions with an electron mask was shown in Figure 22. The Laplace solution for this double disk geometry was given by Sherman and Parker (1970) and can be characterized by the following parameters:

ratio of disk radii, $\alpha = r_o/r_e$

ratio of potentials, $\gamma = \phi_o/\phi_e$

43

Since the attracting potential, Φ_0, is positive and the electron mask potential is negative it is possible that the potential along the stagnation line can become negative and repell the negative ions. Sherman and Parker show that the critical value of γ is given by

$$-\gamma_c = \frac{\sqrt{1 - \alpha^2}}{1 - \sqrt{1 - \alpha^2}}$$

and is shown in Figure 23. If $|\gamma| > |\gamma_c|$ there is no repelling potential and for $|\gamma| < |\gamma_c|$ the potential becomes negative somewhere along the stagnation line. The variation of the potential along the stagnation line from the analytic result will be compared to the finite difference solution used in the Monte Carlo iteration procedure.

The Monte Carlo calculations for the negative ion collection in the collision-less and large Debye number limit were performed for the following choice of parameters.

$$\frac{\lambda_\infty}{D} = 1000$$

$$\frac{\lambda_D}{D} = 1000$$

$$S = 3.10$$

$$\alpha = \frac{r_0}{r_e} = 0.50$$

$$\Phi_0 = 200$$

$$\Phi_e = -40 \text{ and } -20$$

The two values of Φ_e gives values of γ equal to

$$\gamma = -5 \text{ and } -10$$

which from Figure 23 indicates a repelling potential for the first value but not for the second. In Figures 24 and 25 the finite difference results along two lines $r = 0$ (stagnation) and $r = R/2$ are shown and compared to the analytic solution. Figure 24 shows excellent agreement for the two results along the

44

CRITICAL POTENTIAL RATIO

$\alpha = r_0/r_e$

$\gamma = \Phi_0/\Phi_e$

$\gamma_c = \dfrac{\sqrt{1-\alpha^2}}{1-\sqrt{1-\alpha^2}}$ (Sherman and Parker, 1970)

$|\gamma| > |\gamma_c|$ NO REPELLING POTENTIAL

$|\gamma| < |\gamma_c|$
REPELLING POTENTIAL

$-\gamma_c$

100

10

1

0   .2   .4   .6   .8   1.0

α

FIGURE 23

45

PRESENT FINITE ○ $r = 0$
DIFFERENCE ● $r = R/2$
RESULTS

$\phi_o = 200 \qquad r_o = R/2$

$\phi_e = -40 \qquad r_e = R$

$\gamma = \dfrac{\phi_o}{\phi_e} = -5$

ANALYTIC SOLUTION
FOR $r = 0$ (SHERMAN
AND PARKER, 1970)

$\alpha = \dfrac{r_o}{r_e} = 0.50$

ϕ

$\dfrac{X}{R}$

FIGURE 24

PRESENT FINITE
DIFFERENCE
RESULTS

○ $r = 0$
● $r = R/2$

ANALYTIC SOLUTION
FOR $r = 0$
(SHERMAN AND
PARKER, 1970)

$\Phi_0 = 200 \qquad r_0 = R/2$

$\Phi_e = -20 \qquad r_e = R$

$\gamma = \dfrac{\Phi_0}{\Phi_e} = -10.0$

$\alpha = \dfrac{r_0}{r_e} = 0.50$

Φ

60

40

20

0

-20

-40

0.5   1.0   1.5   2.0   2.5   3.0   3.5

$\dfrac{X}{R}$
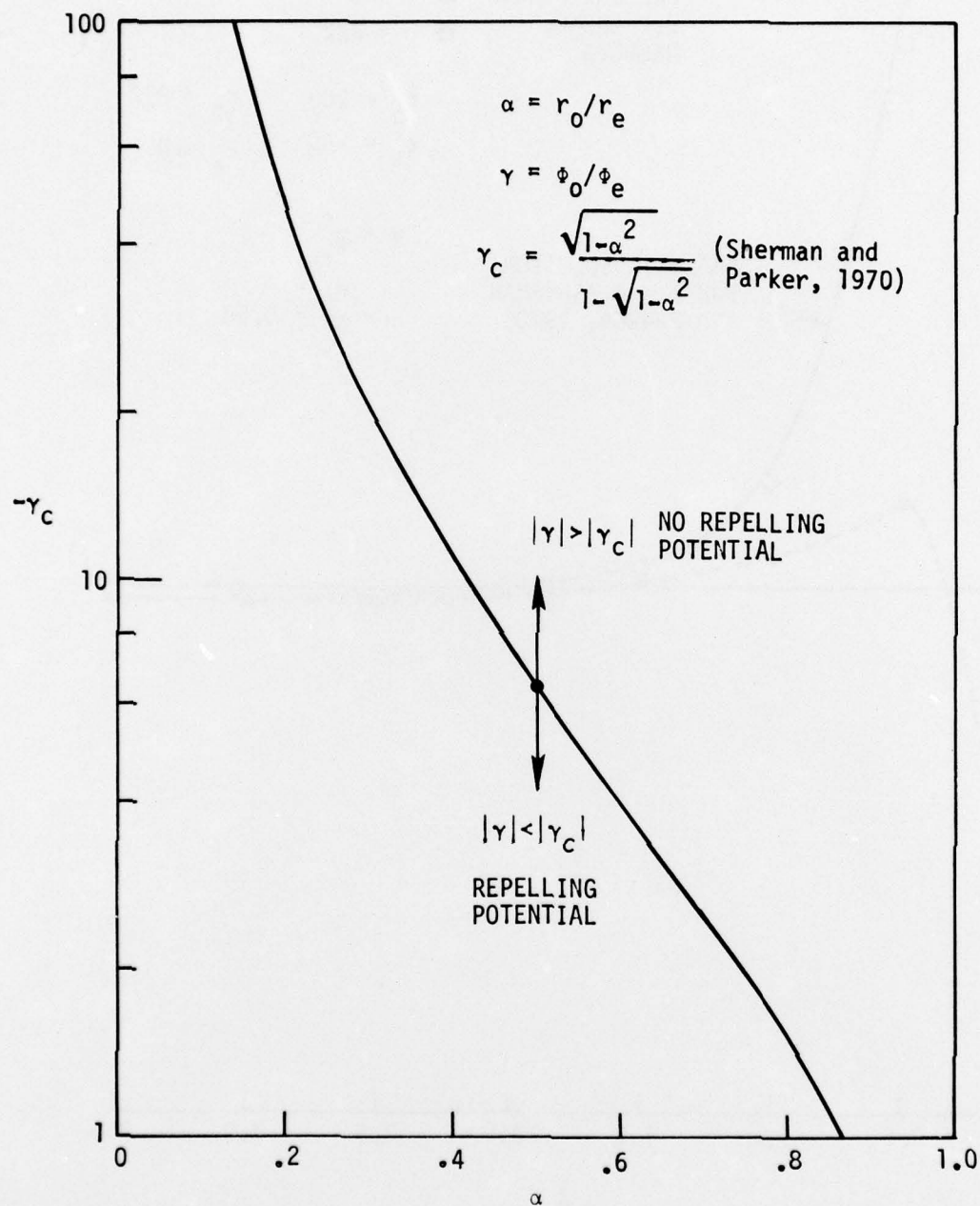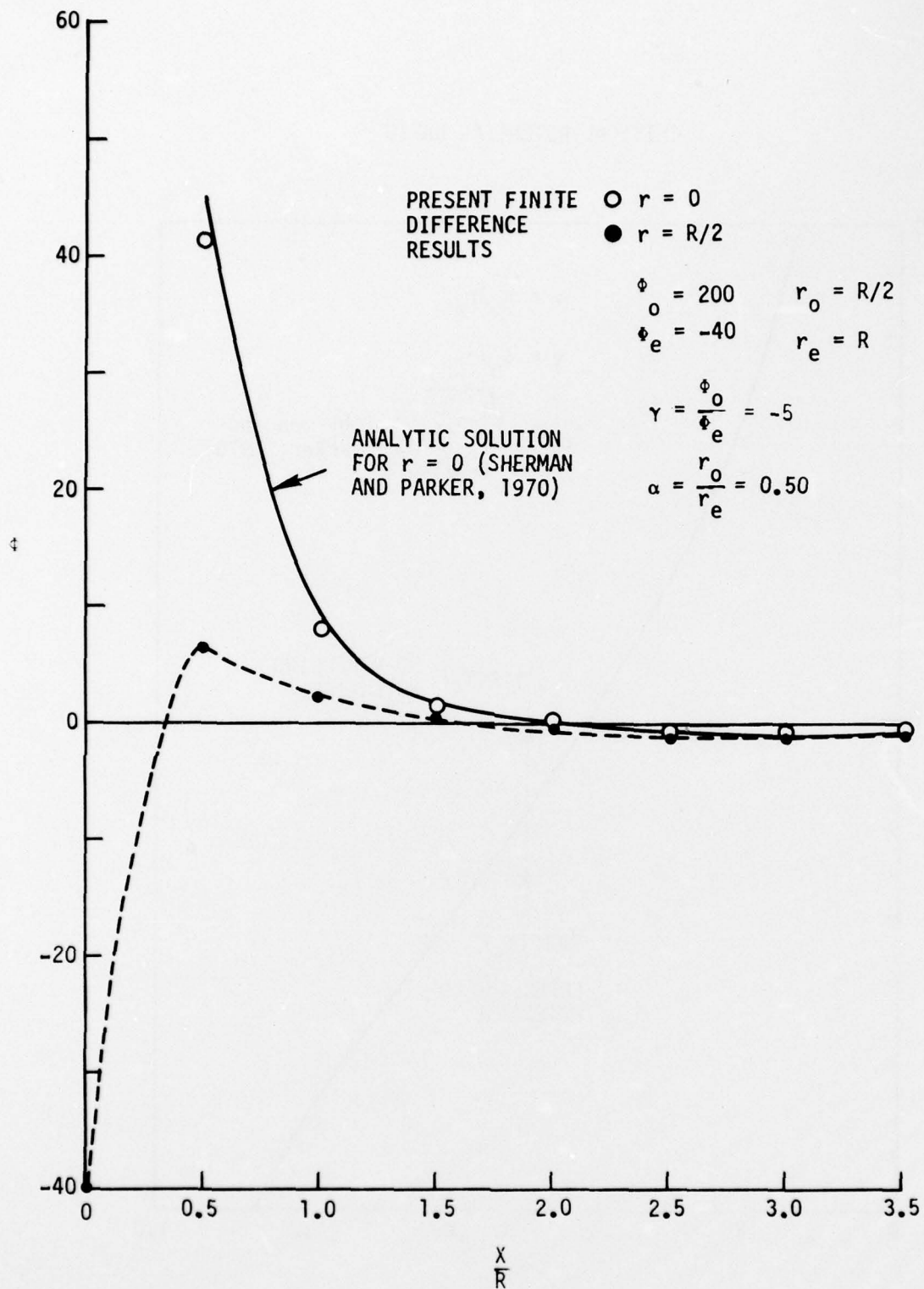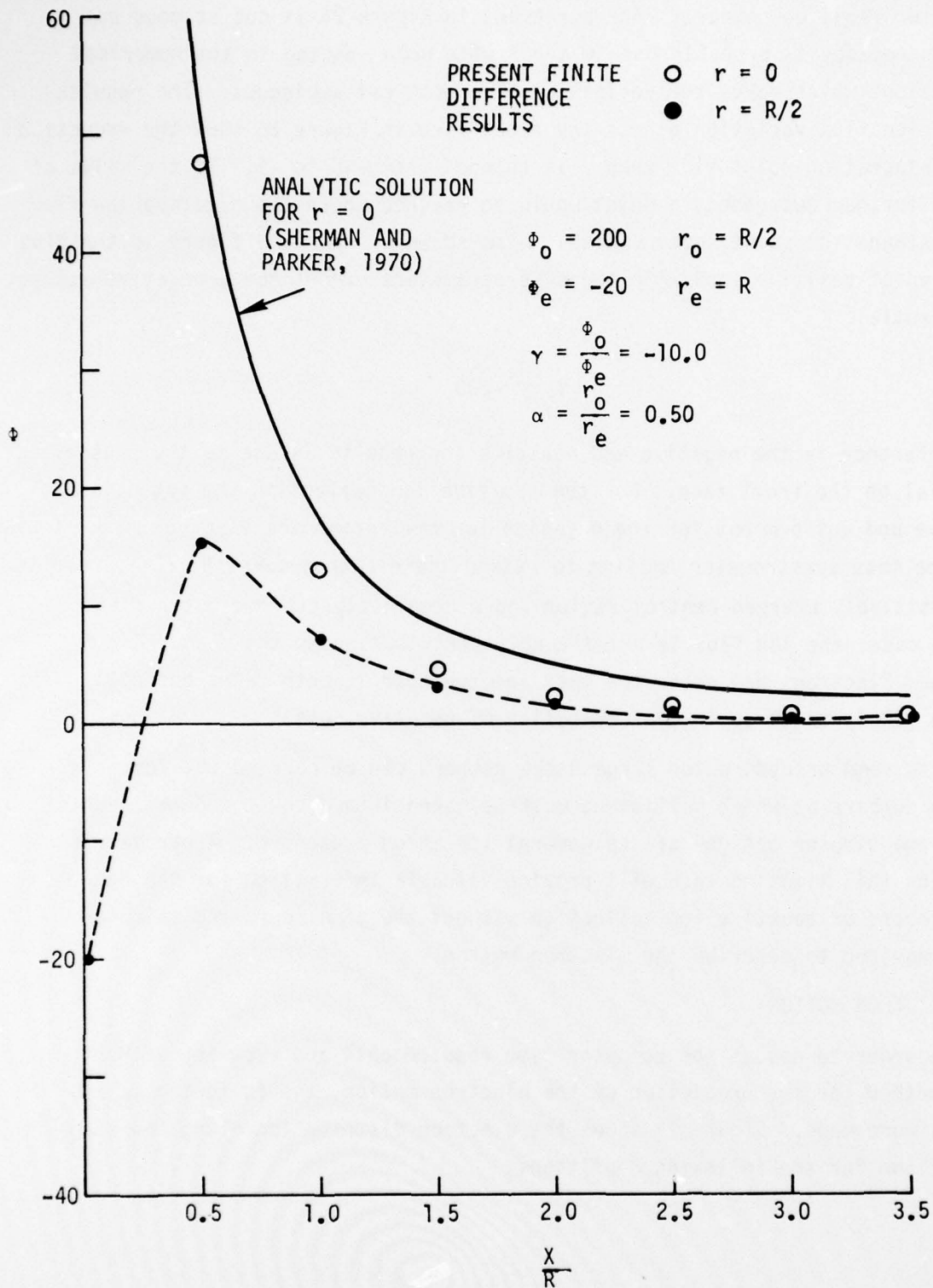
FIGURE 25

stagnation line where both show a change in sign of the potential at approximately two radii downstream. The agreement in Figure 25 is not as good but this discrepancy is probably due to the finite node spacing in the numerical calculations which makes the definition of α somewhat ambiguous. The results for the ion flux variation across the front face in Figure 26 show the reduction of the stagnation point flux when γ is changed from -10 to -5. If the value of $|\gamma|$ was further decreased, a point would be reached where the negative ion flux at the stagnation point would vanish. Also shown on the same figure is the flux variation of positive ions with the same parameters except for a negative attracting potential.
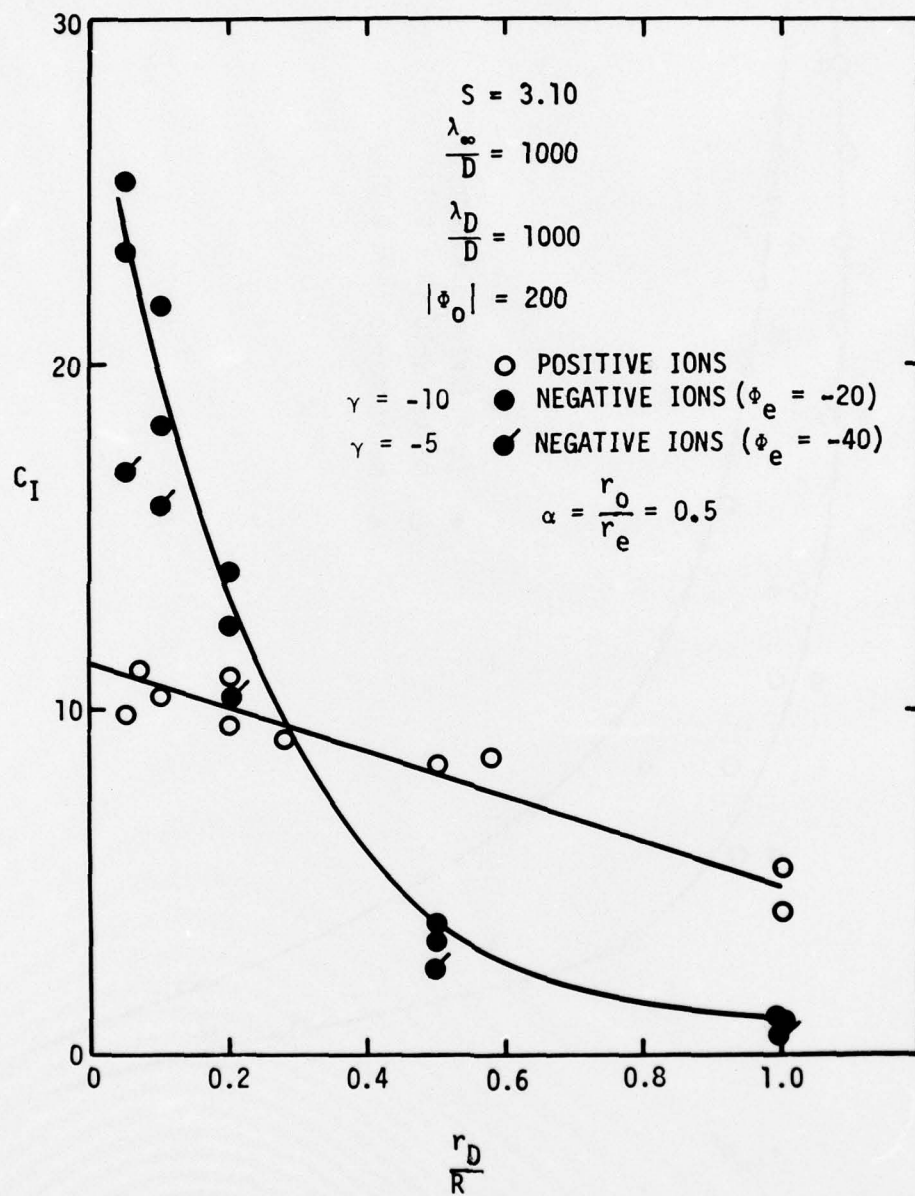
$$\phi_0 = -200$$

The difference in the negative and positive ion results is due to the prescribed potential on the front face. For the positive ion collection the potential is negative and uniform but for the negative ion collection the electron mask is placed over the mass spectrometer housing to retard the electron current. This results in a positively charged central region and a negatively charged outer disk. In both cases the ion flux is not the only contribution to the measured current. Electrons may enter the mass spectrometer in both cases but will be more likely to do so in the collection of negative ions.

This same procedure for large Debye numbers can be carried out for Knudsen numbers at which collisions must be taken into account and represents one of the simpler options of the general iteration procedure. A parametric study for this limiting case will provide valuable information for the general process of negative ion collection without the time consuming calculations required to describe the electron motion.

7.2 ELECTRON MOTION

In order to assess the computer time requirements and accuracy of Monte Carlo method for the prediction of the electron motion, the following calculations were made. Figure 27 shows the electron distribution along the stagnation line for the following conditions;

48

FIGURE 26

POSITIVE AND NEGATIVE ION FLUX VARIATION ACROSS COLLECTING PLATE

$S = 3.10$

$\frac{\lambda_\infty}{D} = 1000$

$\frac{\lambda_D}{D} = 1000$

$|\Phi_0| = 200$

○ POSITIVE IONS

$\gamma = -10$ ● NEGATIVE IONS ($\Phi_e = -20$)

$\gamma = -5$ ◖ NEGATIVE IONS ($\Phi_e = -40$)

$\alpha = \frac{r_0}{r_e} = 0.5$

ELECTRON DISTRIBUTION ALONG STAGNATION LINE

- Equilibrium Electron Gas
- Monte Carlo (S = 0.1)
- Monte Carlo (S = 0.014)
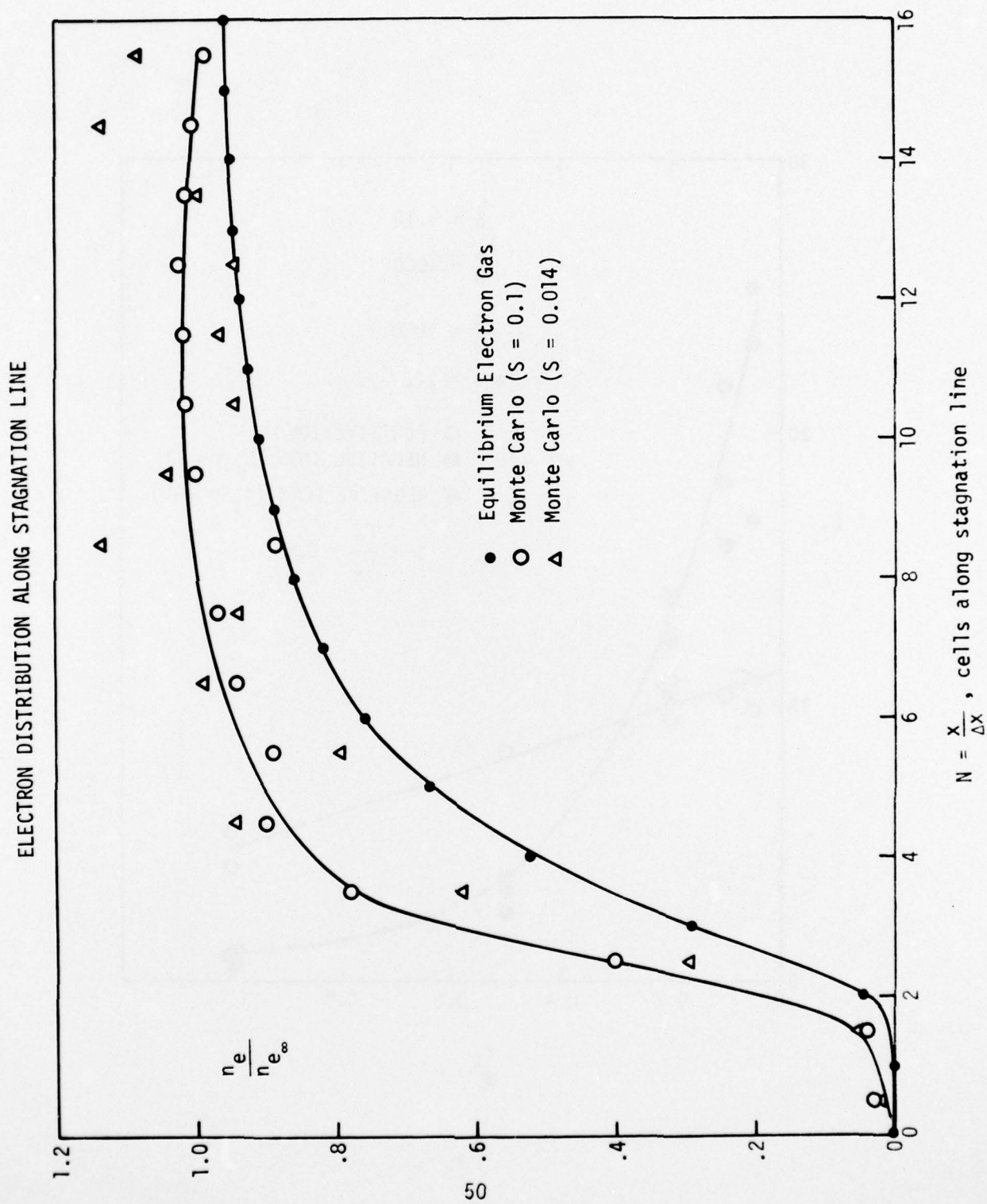
$N = \dfrac{x}{\Delta x}$, cells along stagnation line

FIGURE 27

Collisionless flow $\lambda_\infty/D \gg 1$

Large Debye number $\lambda_D/D \gg 1$

Negative Potential $\phi_0 = -200$ (uniform across front face)

In the calculations for the collection of positive ions, the electrons were assumed to be in Boltzmann equilibrium for large negative front face potentials. For the calculations shown in this figure the Monte Carlo calculations for the electrons are compare favorably/with the results of the equilibrium electron gas assumption. The electron speed ratios for the calculations were taken to be 0.10 and 0.014 corresponding to ion speed ratios of 24 and 3.4, respectively. The two results for these speed ratios are similar enough to conclude that for very small speed ratios the electron motion is independent of speed ratio for a repulsive potential. The increased scatter in the results for a speed ratio of 0.014 is due to the smaller movement time interval for a fixed time step, i.e., the calculation for the smaller speed ratio represents a shorter simulation time. Since the larger speed ratio calculation converges faster, it would be useful to determine the largest speed ratio for the given conditions which results in a solution independent of the speed ratio.

Another series of Monte Carlo calculations were made to determine the requirements to predict the electron motion for a positive, attractive front face potential. For these calculations the flow was again assumed collisionless, the Debye number large enough for the Laplace solution to be valid and the front face at a non dimensional potential equal to 200. No electron mask was placed over the front face and the purpose of these calculations was to properly simulate the electron motion with an attractive field. Figures 28 through 30 show the potential distribution, number density and velocity along the stagnation line. In the collisionless case, the electrical energy and kinetic energy of the electron are directly related as shown in Figures 28 and 30. A number of calculations were made for various values of, Δtm, the movement time interval. The value shown on the figures was found to be close to optimum between the larger values which led to convective errors and smaller values which required excessive computer time to reach a steady state.

51

VARIATION OF ELECTRIC POTENTIAL

$$\frac{\lambda_D}{D} = 1000$$

$$\frac{\lambda_\infty}{D} = 1000$$

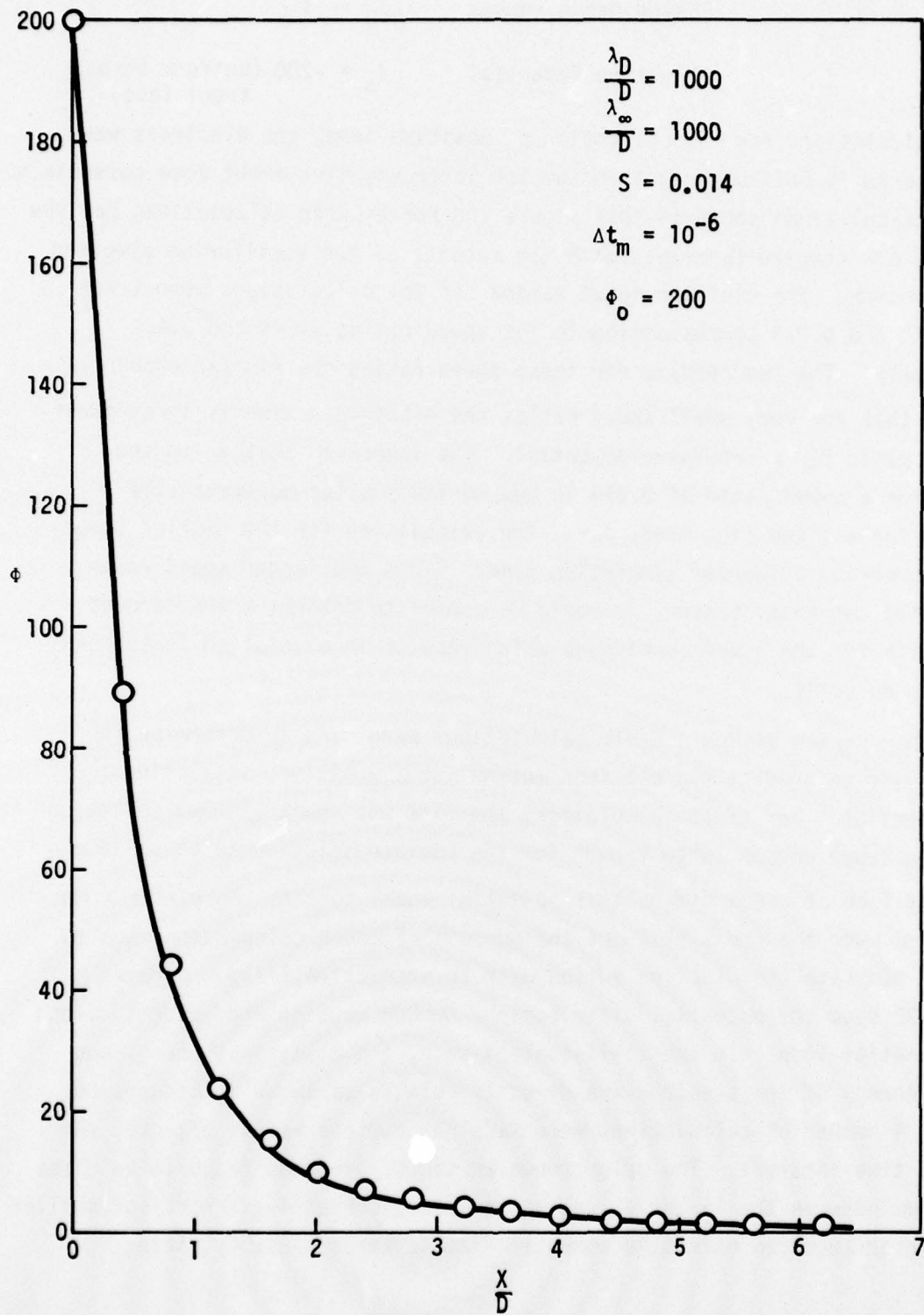$$S = 0.014$$

$$\Delta t_m = 10^{-6}$$

$$\Phi_o = 200$$

FIGURE 28

ELECTRON NUMBER DENSITY

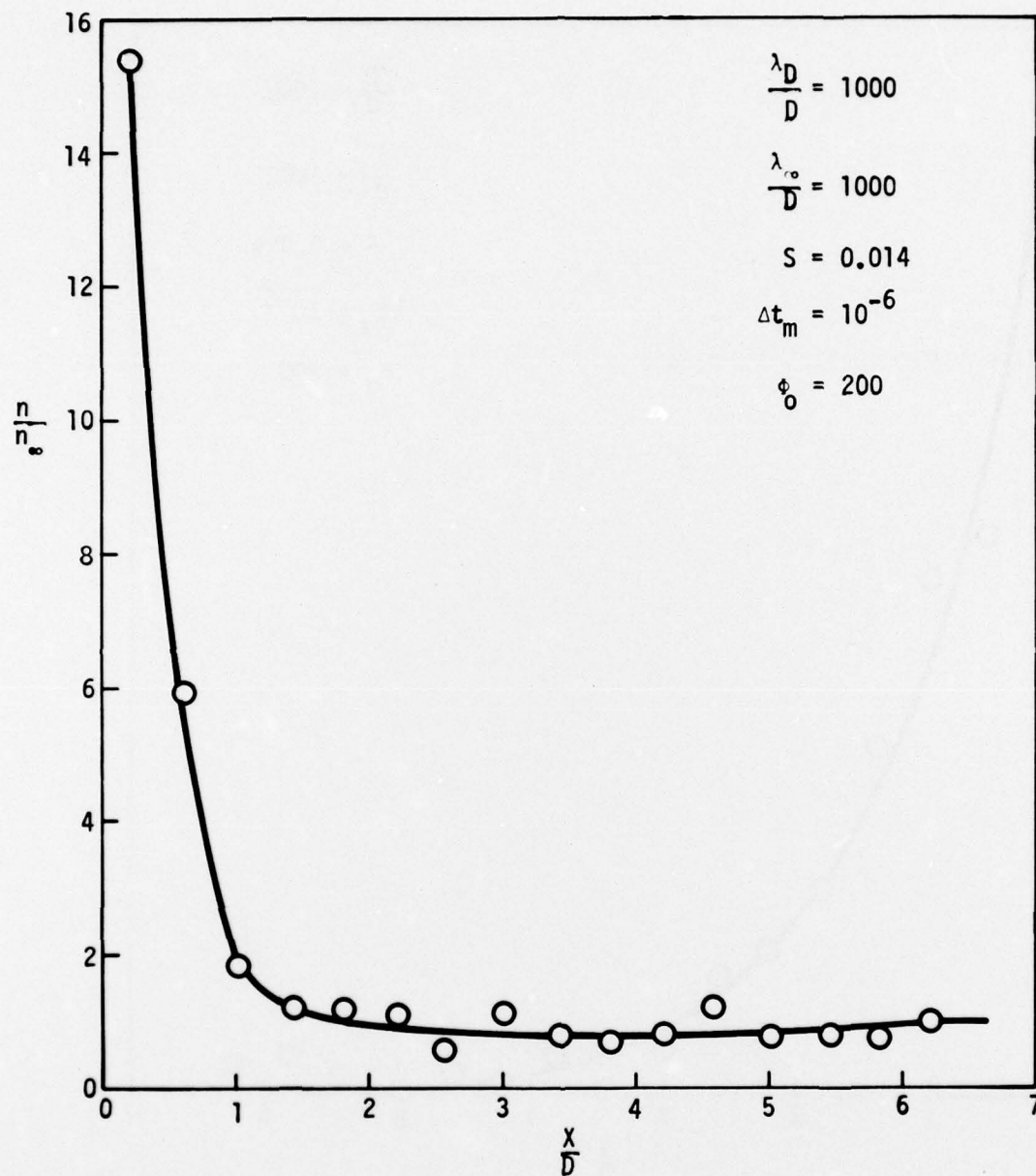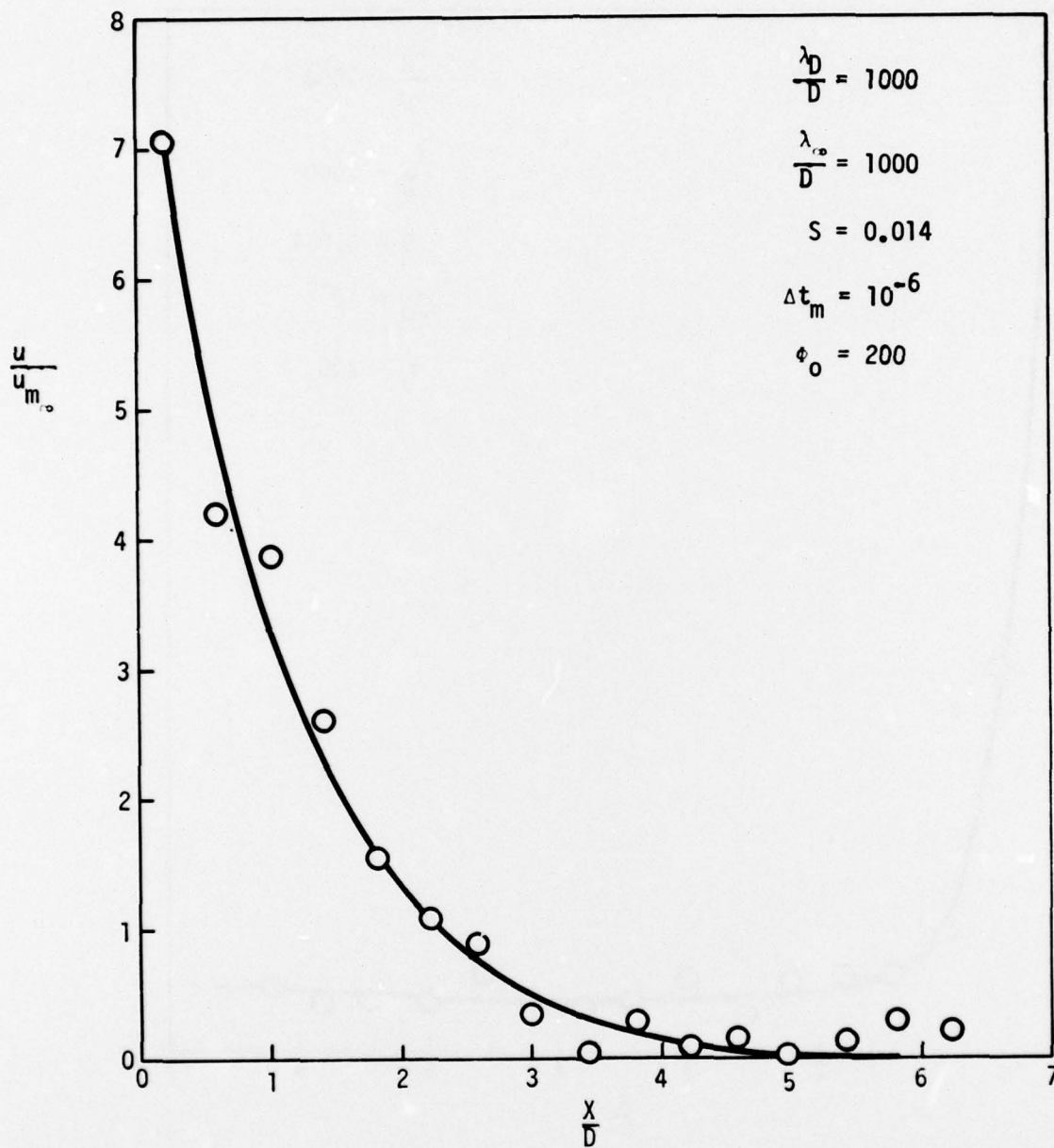

FIGURE 29

ELECTRON VELOCITY

FIGURE 30

8. CONCLUSIONS

The results of the systematic parameter study for the collection of positive
ions were discussed in Section 2. Most of the important collection variables
were investigated over appropriate ranges of interest. Additional parameters
such as the effects of vehicle angle of attack and the molecular internal
degrees of freedom were examined. However, only a few calculations were made
to assess the effects of relaxing the original assumptions, e.g., zero angle
of attack and neglect of the internal degrees of freedom. Results of the
angle of attack calculations indicate that the flux coefficient is only
slightly affected, on the order of 10%, for moderate angles of attack, e.g.
less than 20 degrees. The effects of rotational energy was also formed to be
about a 10% effect for the flow conditions considered. Further work for the
positive ion collection should include a systematic study of these effects
and the role of chemical reactions on the collection process.

The formulation for collection of negative ions has been completed and the
preliminary calculations indicate that the electrons are described properly.
Calculations completed for the negative ion flux in the collisionless limit
for large Debye numbers will be continued and extended into the transition
regime.

REFERENCES

Jeans, J. H., An Introduction to the Kinetic Theory of Gases, Cambridge University Press, 1940.

Narcisi, R. S., "Composition Studies of the Lower Ionosphere," AFCRL, Based on Four Lectures Presented at the International School of Atmospheric Physics, Erice, Sicily, June 1970.

Sherman, C. and Parker, L. W., "Potential Due to a Circular Double Disk," AFCRL-70-0568, Air Force Cambridge Research Lab., Bedford, Massachusetts, 12 October 1970 (also Journal of Applied Physics, Vol. 42, No. 2, February 1971).

Sonin, A. A., "Theory of Ion Collection by a Supersonic Atmospheric Sounding Rocket," Jour. Geophysical Res., Vol. 72, No. 17, September 1967.

Sugimura, T. and Vogenitz, F. W., "Monte Carlo Simulation of Ion Collection by a Rocket-Borne Mass Spectrometer for Collisionless and Transitional Flowfields," Technical Report TR-73-0448, Air Force Cambridge Research Lab, Bedford, Mass., July 1973.

Sugimura, T. and Vogenitz, F. W., "Monte Carlo Simulation of Ion Collection by a Rocket-Borne Mass Spectrometer," Jour. Geophysical Res., Vol. 80, No. 4, February 1975.

Sugimura, T., "Monte Carlo Simulation of Ion Collection by a Rocket-Borne Mass Spectrometer, Scientific Rep. No. 1," AFCRL-TR-75-0240, Air Force Cambridge Res. Lab., Bedford, Mass., February 1975.

Sugimura, T., "Prediction of Positive Ion Collection by a Rocket-Borne Mass Spectrometer," presented at 10th International Symposium on Rarefied Gas Dynamics, Aspen, Colo., July, 1976. (accepted for publication in the proceedings)

Vogenitz, F. W., "Computer Simulation of Ion Collection by an Ionospheric Probe," AFCRL-TR-0006, 1 January 1973.